Accuracy of radial-velocity measurements for early-type stars

II. Investigations of spectrum mismatch from high-resolution observations

R.E.M. Griffin[*,**]**, M. David, and W. Verschueren**[***]

Astrophysics Research Group, University of Antwerp (RUCA), Groenenborgerlaan 171, B-2020 Antwerpen, Belgium

Abstract. The accuracy with which radial velocities of early-type stars can be measured is limited in practice by the existence of asymmetrical differences between object and template spectrum, constituting "spectrum mismatch". Our studies of the magnitude of spectrum-mismatch errors, commenced in Paper I (Verschueren et al. 1999) on the basis of synthetic spectra having different attributes of effective temperature ($T_{\rm eff}$) and $\log g$, are continued here in a complementary approach that employs *observed* spectra. From over 60 de-archived observations we derive accurate wavelength scales for the spectra of 16 dwarfs of spectral types B8−F7, and examine the results of cross-correlating the spectra against different (observed) template spectra. We also test the effects of (a) truncating the spectra at different levels below the continuum, (b) adding rotational broadening to enforce a *visual* match of line-width between object and template, (c) applying rotational broadening to exacerbate a rotational mismatch, and (d) neglecting the presence of faint companion spectra. We also cross-correlate pairs of spectra such that the differences between their $T_{\rm eff}$ are minimal. We conclude that it will be possible to measure radial velocities to an accuracy considerably better than 1 km s^{-1} for slowly-rotating stars in the range of spectral types examined, and a careful discussion of the nature and sources of the random and systematic errors that become significant in work of this nature enables us to specify conditions that are important for achieving such accuracy routinely. We find that both rotational broadening, and the star-to-star variations in line strengths that are so prevalent among A-type spectra, can give rise to more deleterious mismatch shifts (RV errors) than do differences in $T_{\rm eff}$ alone, even for $\Delta T_{\rm eff}$ as great as $300 - 400$ K. By intercomparing the results given by wide regions of spectrum ($\sim$800 Å) with those obtained by isolating small groups of features in very narrow windows ($\sim$30 Å), we have been able to designate a window near $\lambda\,4570$ Å that should be particularly reliable for high-accuracy results, and we propose further studies at very high S/N ratio in that specific window to complement and extend the results of the present paper.

Key words: techniques: radial velocities — techniques: spectroscopic — stars: early-type

Send offprint requests to: R.E.M. Griffin,
e-mail: remg@astro.ox.ac.uk
 [*] One-time Visiting Professor, R.U.C.A.
 [**] *Present address*: c/o Department of Nuclear & Astrophysics, University of Oxford, 1 Keble Road, Oxford, OX1 3RH, UK
[***] Former Postdoctoral Fellow of the Fund for Scientific Research, Flanders-Belgium (F.W.O.).

1. Introduction

The aim of this project is to define a scheme for determining radial velocities (RVs) of hot (O-B-A) stars to within specified accuracy (systematic errors) and precision (random errors). In this series of papers we investigate the origins of *systematic* errors from different angles, and discuss methodologies to minimize them. Specific problems relating to *random* errors in RVs for early-type stars have already been discussed by Verschueren & David (1999).

It has become routine practice to measure RVs by cross-correlating the spectrum of a programme object against a reasonably similar physical template or mask, whose own velocity is either known absolutely or is determined relative to a fiducial spectrum. The incorporation of this principle into machinery gave birth to the Cambridge "radial-velocity spectrometer" (Griffin 1967) and to an assortment of "CORAVEL"-type instruments which followed it (e.g. Griffin & Gunn 1974; Baranne et al. 1979; Fletcher et al. 1982). In a further refinement, the physical template in such an instrument is replaced with a digital one (e.g. Latham & Stefanik 1992; Baranne et al. 1996). Most of

the current effort in that activity is going into velocity determinations of stars of solar types and cooler, which are particularly suitable for such equipment. However, there are pressing astrophysical needs for rapid and plentiful accurate velocities for hotter stars too, as discussed by Verschueren (1991). Improved proficiency with numerical masks has encouraged pilot studies of cross-correlation characteristics for early-type stars. Morse et al. (1991), for instance, investigated whether the systematic errors caused by object-template mismatch in both spectral type and rotational velocity could be held under 1 km s^{-1} for narrow-lined stars and under 2 km s^{-1} for rapid rotators if appropriate low-frequency filtering were applied. Increasing pressure to achieve a routine working accuracy better than 1 km s^{-1} for early-type stars has spurred attempts to improve on the level achieved by Morse et al., both by variations of their technique and by closer investigation of details.

The first paper in this series (Verschueren et al. 1999; hereinafter called Paper I) investigates, via numerical experiments, the factors which affect the level of accuracy that is nominally attainable for radial-velocity measurements of A-type stars by cross-correlation. Differences ("spectrum mismatch") between object and template can cause systematic errors, and are particularly prevalent in early-type stars where Nature provides rather few lines and many striking differences in spectral features between stars of nominally similar T_{eff} and $\log g$. The present paper is a continuation of those experiments, but sets out from a somewhat different angle and is therefore parallel to, rather than an extension of, Paper I.

Spectrum mismatch errors are liable to occur whenever blending lines in an object and a template spectrum differ in relative strength. The asymmetry affects systematically the shape of the cross-correlation function (CCF), thereby introducing corresponding errors into the location of its maximum (i.e. the measured RV). Each of the many variable characteristics in a stellar atmosphere – temperature, luminosity and metallicity are rather obvious ones – is therefore capable in principle of contributing a systematic error to a measured RV.

In late-type stars the richness and family likeness of lines available for RV measurement far outweigh the instances of serious differences or deleterious blends, but in early-type spectra that ratio falls well below a critical value. The changeover occurs near the late-A/early-F border, depending on rotational velocity and spectral peculiarity: a late Am star can be measured for RV with a K-type mask in a CORAVEL instrument; the orbit of the double-Am binary HD 177390/1 (Griffin 1988), for instance, was based on measurements from 4 different CORAVEL-type instruments all employing a physical K-type mask derived from the spectrum of Arcturus. For early types in general, the shortage of conforming features requires balancing the need to include as many lines as possible against the need to avoid lines which would

contribute systematic errors greater than the expected random errors.

In view of the relatively frequent and often highly bizarre spectroscopic peculiarities to which stars in the temperature range $\sim 15\,000 - 7\,000$ K (types B−F) seem particularly prone, it is necessary to examine the errors contributed by different spectral regions, and to define suitable spectral windows to eliminate specific features or regions where necessary. In Paper I we generated a grid of noise-free synthetic spectra corresponding to late B– early F dwarfs and sub-dwarfs and cross-correlated pairs, allowing T_{eff} and $\log g$ to vary within specified limits for selections of v_{rot} between 0 and 300 km s^{-1}. By thus maintaining tight control over the production of differential asymmetries from those causes, we were able to establish the basic levels of RV errors from spectrum mismatch.

Real spectra, however, are complicated by additional problems which standard model stellar atmospheres do not address, so the experiments with synthetic spectra contributed a very necessary but not a sufficient set of results. In the present paper (Paper II) we investigate a similar sub-set of stellar types and luminosities but proceed from observed stellar spectra, with a view to examining the influences of individual idiosyncrasies. The compass of this study is therefore broader than that of Paper I, though its borders are less stringently defined. Inevitably, because real spectra are not noise-free, this study is also slightly less decisive. When spectral lines are blurred by rotation, or when they are naturally weak, the contrast of the CCF is reduced and the noise proportionally increased. In this paper we have largely circumvented the first of those problems by selecting stars with sharp-lined spectra (≤ 30 km s^{-1} projected rotation).

We first discuss the problems from the perspective of an observational approach (Sect. 2), and describe the methods and techniques we adopt to meet the technical challenges which they present (Sect. 3). In Sect. 4 we describe cross-correlations of pairs of spectra through a variety of wavelength intervals, justify the techniques we adopt, and examine the associated errors. In Sect. 5 we assess the trends we find, and offer in Sect. 6 some practical suggestions for the continuation of studies on the design of a programme of radial-velocity measurements.

2. An observational approach to the problem

A star's T_{eff} and $\log g$ are globally summarized in its spectral-type and luminosity classification. Early-type spectra, in particular, also display quite striking differences in a number of other parameters besides T_{eff}, $\log g$ and v_{rot}. Actually there may even be some doubt as to the precise effect of $\log g$ upon an early-type absorption spectrum; Jaschek & Gómez (1998) compared the luminosity classes of early-type stars given by highly experienced classifiers on the one hand and the absolute

magnitudes derived from Hipparcos parallaxes on the other, and drew the somewhat disconcerting conclusion that the assigned luminosity classes do not necessarily correspond monotonically to absolute magnitude. In view of the extensive individuality of early-type stars, it is possible that what is routinely interpreted as a sequence in $\log g$ alone is in reality a convolution of effects that mutually mask or reinforce one another. However, our understanding of the subtle yet (in this context) crucial effects of other astrophysical variants is still largely phenomenological, and so can only be examined in *observed* spectra. The causes and significance of the chief factors besides $T_{\rm eff}$ and $\log g$ are mentioned in turn below.

2.1. Chemical peculiarities

The characteristic and very different traits manifested by stars branded as "chemically peculiar" (CP) are central to the kinds of mismatch which are by no means uncommon in stellar spectra of this temperature range. The differences in appearance (e.g. in lines of Ca II, Si II, Cr II, rare-earths) often far outweigh the changes in line strengths due to modifications in $T_{\rm eff}$ or $\log g$. Enhancements of such lines will therefore cause problems for RV measurements whenever they happen to be closely blended with lines of Ti II or Fe II which are common to the same spectra.

2.2. Rotation

The main deleterious effect caused by stellar rotation is increased blending, leading to a loss of distinction between lines which would give accurate RV measurements and others which are responsible for mismatch shifts between two dissimilar stars. Mismatch errors therefore become increasingly unavoidable (see Paper I). The broader, shallower lines resulting from increased rotation cause a reduced contrast in the CCF, with a concomitant increase in random errors. Another somewhat more subtle effect occasioned by increasing rotation is a reduction in the observable convective line-shift (see Sect. 2.3). Other second-order rotationally-dependent influences can cause changes in the basic shapes of lines. For example, if a rapidly-rotating star is viewed nearly pole-on, its decreased surface equatorial temperature causes the emergent profiles of weak lines to be square or trapezoidal rather than Gaussian (Gulliver et al. 1991), giving rise to somewhat ill-defined line centroids and correspondingly raised uncertainties in the CCF. Since the inclination i of a single star is not known, such effects are likely to be overlooked unless the spectra in question are examined at very high resolution. The loss of distinction of individual lines brought about by rotation also presents a particular problem with the determination of wavelength scales by the "zero-velocity" method used here (see Sect. 3.5).

2.3. Stellar granulation

Stellar surfaces are patterned by small-scale velocity fields or granulation, in which hot, rising (emitting) pockets of material are interspersed with cooler, sinking (absorbing) ones. Slightly different velocities therefore tend to dominate in different layers of the line-forming region of an atmosphere, giving rise to small, characteristic distortions in line profiles. In the Sun, the bisector of a "typical" line of intermediate strength and excitation potential is C-shaped and has a maximum blue-shift of about $300~\rm ms^{-1}$ (Dravins 1999). If a magnetic field is present, the granules are smaller and cause correspondingly weaker distortions. With increasing rotation the asymmetry decreases, the position of the centroid tending towards the small nett shift (bluewards for solar-type stars) corresponding to the statistical bias of hot, rising elements (Dravins 1985).

Though one can (and, to some extent, has to) generalize about the effects of stellar granulation, its behaviour seems to be fairly individualistic and to depend upon the vigor of a star's surface convection, or upon variations in magnetic field-strength with rotation. On the surface of the Sun the degree of line-asymmetry is reduced in sunspot regions, and similar anti-correlations with changes in magnetic-field strength are expected to occur on other stars too. Such changes have indeed been detected in stellar spectra; Toner & Gray (1998) measured the modulation in a line-bisector in the spectrum of the chromospherically-active G8 dwarf ξ Boo. According to high-resolution observations and line-profile modelling of early A stars by Landstreet (1998), certain trends in the granulation effects in non-magnetic stars are predictable. The magnitude of the distortions depends upon temperature (and possibly upon spectral peculiarity), and increases quite dramatically towards the F class; in individual sharp-lined A2m and A5m stars bisectors can be curved asymmetrically in an *anti*-C, with a span of about $1~\rm km\,s^{-1}$. The intrinsic shape of the bisector affects the position of the line centroid, and although the distortions will not themselves be resolved at the resolutions typical of radial-velocity spectrometers their effects will nevertheless impinge upon the RV measurements that depend upon those lines. The presence of these highly individualistic line-profile distortions therefore represents one lower limit to the *accuracy* of current RV measurements of stars in which surface convection is significant. Studies of line asymmetries in stars are still in their infancy, and as yet there is little general information on changes in the asymmetry patterns. If the velocity pattern causing the line asymmetries is static, it will cause a constant offset from the true value; if it fluctuates periodically, the corresponding changes in centroid position will mimic displacements that could be ascribed to a stellar planet.

2.4. Other causes of anisotropy and inhomogeneity

Many of the physical characteristics of these hot stellar atmospheres – stratification, vertical diffusion of elements, horizontal concentrations of material – can influence the small-scale symmetry, and hence the observed centroid, of an absorption line.

(i) Stratification and diffusion. Vertical stratification of material is suspected in slowly-rotating stars (which seem to be dominated, as a group, by Am and CP classes). Since the formation of a strong feature encompasses a large vertical depth of an atmosphere in which stratification may be pronounced, a line such as the Ca II K line is unlikely to be reliable for accurate RV determinations, however tempting it may seem; in Vega, for instance, it even appears slightly asymmetrical in the core. If diffusion has operated within the line-forming region, weak lines of different elements might show small mutual displacements reflecting the different small-scale turbulence representative of different heights, but such shifts have not yet been detected, or even sought, as far as we are aware.

(ii) CP stars show isolated condensations associated with surface spots. Abundance inhomogeneities on quiescent stars will tend to cancel if the characteristic areas of their distributions are small compared to the radius of the star; however, on CP stars the active spots are characteristically large and few, and impart signatures of their longitudinal velocity components (i.e. RV shifts) in their line centroids.

(iii) Gross effects such as stellar winds and mass outflow tend to be most pronounced in the strongest lines (e.g. Balmer lines) whose cores are formed at high levels of the atmosphere where the disturbing events are seated. Those lines are therefore likely to be unreliable for stellar RV measurements, especially in (super)giants, except as a last resort – for instance when other lines are too diffuse, as in cases of rapid rotation – though at the cost of lower accuracy.

2.5. Binary membership

There is no astrophysical reason to exclude from this project a member of a spectroscopic binary. That would impose almost impossibly tight restrictions on the choice of spectra if implemented rigorously; faint companions to even quite bright stars are still being discovered (e.g. HR 104, Hill et al. 1993). We do indeed include binary systems in the sample selected for this paper (Table 1). However, the possibility of interference from a secondary spectrum, if it is also of early type, is of course very real, so it is necessary to impose suitable restrictions, e.g. truncating the spectrum at a certain distance below the continuum, in order to avoid or minimize such interference.

2.6. Interstellar absorption

Owing to the presence of sharp IS features within the core of the K line in many early-type stars, the Ca II K line is unsuitable for these studies except where stars are sufficiently nearby that IS contributions are negligible.

2.7. Effects of observational selection

Our sample of sharp-lined late-B and early-A stars that are bright enough for high-dispersion observations can be criticized as observationally biased. It is frequently claimed that Am and CP stars have intrinsically sharp-lined spectra, though the statistics are sensitive to observational selection because proving the validity of the converse, namely that spectra whose lines are seriously washed out through rotation definitely do *not* show fine abundance peculiarities, is extremely challenging. Not only does the demand for increased S/N rise along with rotational velocity, but the problems of blending (i.e. line blurring) become so acute that they can only be handled by spectrum synthesis, thereby relying on the same basic foreknowledge about the individual star which is *ipso facto* being sought. Even Sirius and Vega, the two brightest A dwarfs in the northern sky and whose spectra have easily the highest S/N ratios in our sample (see Table 1), are "abnormal". Sirius is classified as mild Am. Vega – once the universal standard for A-type dwarf spectra – has lines that are almost as narrow as those of Sirius, but is somewhat metal-poor; moreover, at high dispersions its line profiles show clear abnormalities to the extent that we were obliged to reject this "standard" star as a potential template for the purposes of this paper.

Although the present study is necessarily limited to, and possibly restricted by, the types of spectral peculiarity exhibited by those stars for which suitable observational material was available (see Sect. 3.2), the range is sufficient to support a broad attack on the associated problems.

3. Preparing accurate spectra from observations

In this section we describe the generation of wavelength-calibrated spectra from the observations, and discuss aspects of their derivation which impinge upon the accuracy and precision of their wavelength scales.

The observed spectra to be used in these experiments must have wavelength scales that are more accurate (i.e. have smaller systematic errors) than the likely mismatch errors that we propose to investigate. However, the extraction of spectra from observations can introduce extraneous errors of *technical* (instrumental and processing) origin. We therefore focus first on those sources, and describe our attempts to minimize, if not altogether eliminate, the attendant errors. We address the question of absolute stellar RVs here, also. We aim to reduce all

controllable errors in these spectra to less than 0.1 or 0.2 km s^{-1} (< 3 mÅ at $\lambda\,4200$ Å).

3.1. Instrumental characteristics

In order to satisfy the project's demands for variety and wealth of spectroscopic features (which in early-type stars implies a wide wavelength range), we require a large, homogeneous set of high-resolution, high-S/N spectra representing a broad selection of early-type stars, all with accurately-known absolute velocities. The greater the resolution, the better our ability to investigate the effects of blends, provided $v_{\rm rot}$ is also small; a resolving power of 10^5 has the same blurring effect as $v_{\rm rot} = 3$ km s^{-1}. If practical considerations dictate that the spectra have to be observed with different equipment, modes must be selected that are as similar as possible to one another so as to reduce any systematic effects due to differences in resolution, spectral definition or wavelength range; whenever spectral characteristics are not fully shared between object and template, the likelihood of distorting the symmetry or position of the CCF, i.e. of adding systematic error to the RV, is increased.

Despite nominal similarities in resolving power, different spectrographs possess different characteristics of instrumental profile (point-spread function), spectral definition, and fiducial wavelength source ("arc" spectra). If the lines being cross-correlated are isolated and symmetrical and instrumental profiles are symmetrical, small differences in resolution or definition are not expected to contribute errors that are significant for this project. Problems arise when spectral lines are blended, particularly if they are of unequal strength, because the degree of blending will depend both upon instrumental resolution and upon the extent of the wings of the instrumental profile. Moreover, some differential behaviour of those properties with wavelength can be expected since the design of the optical components in the spectrograph will have been optimized optically for a particular wavelength.

The foregoing refers, of course, to the intrinsic properties of a spectrograph, and excludes spectral degradation caused by incorrect focus or spectrum tilt.

3.2. Observational material

Owing to various constraints of time, resources and equipment we have depended upon archived photographic spectra for this project. The wide wavelength coverage and fine pixel size that are characteristic of many photographic spectra (e.g. Griffin 1968; Griffin 1979) render the latter particularly suitable as test material. High S/N can be achieved by co-adding multiple spectra. We chose a wavelength region of $\sim 1\,000$ Å between the Balmer discontinuity and Hβ.

The quantity of such data is in principle vast; in practice, lack of ready access to many plate stores restricted the choice substantially. To minimise the dangers discussed above, we selected spectra mostly from two sources: the Dominion Astrophysical Observatory (DAO) and Calar Alto (CA), and from two specific instrumental combinations: the 96-inch camera and mosaic grating (830 lines mm^{-1}) of the DAO 1.2-m, and the f/12 camera and 632 line mm^{-1} grating of the CA 2.2-m telescope. Both spectrographs offer a maximum reciprocal dispersion near 2.3 Å mm^{-1} in the blue, and in both cases two 10-inch plates are placed end-to-end in the plate holder, thereby admitting a small gap at the exposure centre. Other relevant characteristics are substantially different, however. Intensity calibrations at the DAO are exposed directly onto the plate, whereas at CA one must employ an auxiliary system; at the DAO the relatively small telescope aperture is compensated by an image slicer whose fixed area limits the attainable S/N of a photographic exposure, whereas at CA the conventional entrance slit can be widened to 2.7 mm, and even to twice that, if feasible.

We also used some very high-dispersion spectra (down to 0.75 Å mm^{-1}) of Sirius and Vega taken on IIIa-J emulsion with the Mount Wilson (MW) 100-inch telescope and coudé spectrograph, and intended as material for a spectrophotometric atlas (in preparation). For those spectra the 3$^{\rm rd}$ or 4$^{\rm th}$ orders of the 133B grating (900 lines mm^{-1}) and 114-inch camera had been used. The grain size of the IIIa-J emulsion is almost 3 times smaller than that of the IIa-O emulsion employed at the DAO and CA.

One disadvantage of using archived spectra is an inevitable sacrifice of homogeneity. Fortunately, however, the diversity of the material – dictated by the differing original purposes for which the observations were made – was tolerable. The DAO archive contains the fruits of several programmes designed to study chemical abundances in sharp-lined Bp, Ap and Am types or to monitor RVs of binaries, and includes several fairly homogeneous subsets of sharp-lined spectra. The CA archive is much less extensive; we used a number of high-dispersion spectra of late-B and early-A stars taken by REMG for a programme whose objective was to push the spectral coverage deep into the photographic UV. Few of those plates have the same wavelength coverage.

The selected observations, listed in Table 1, comprise the test spectra which we will cross-correlate in pairs in order to investigate the effects of spectrum mismatch. For each star, the table gives its listed spectral type, source of observation(s) and number of exposures used, its measured $(B - V)$, a suggested temperature derived from its $(B - V)$ (Flower 1996), the S/N ratio, and our estimates of $v \sin i$. Note that the values of $T_{\rm eff}$ given in the Table are *not* spectroscopic derivations, and should not be treated as such. S/N ratios were determined from the noise levels in selected regions of continuum; the values are closely related to the total spectrum width (perpendicular to the

Table 1. Selected spectra

Star	HR	Spectral type[*]	$(B-V)$	T_{eff}[†]	$v\sin i$[§]	Source	No. of spectra	S/N	Wavelength range	Remarks
64 Ori	2130	B8 III/V	−0.11	12 000	5	DAO	1	50	3750−4600	SB2
	8094	B9 V	−0.10	11 700	12	DAO	1	30	3750−4600	SB
	7664	B9p	−0.08	11 100	9	DAO	11	140	3750−4600	SB HgMn
ϕ Her	6023	B9p	−0.07	10 850	10	CA	2	50	3750−4418	SB HgMn
21 Peg	8404	B9.5 V	−0.07	10 850	5 (3.9)	DAO	1	30	3750−4600	
β^2 Cap	7775	B9.5	−0.02	9 850	4	DAO	1	40	3750−4600	SB Hg Mn
o Peg	8641	A1p	−0.02	9 850	8	DAO	13	150	3750−4600	SB HgMn
Vega	7001	A0 V	0.00	9 550	25	MW	9[¶]	300	3750−4600	Unusual line profiles
γ Gem	2421	A0 IV	0.00	9 550	12 (11.3)	CA	2	70	3750−4317	SB
Sirius	2491	A1 V	0.01	9 400	17 (16.5)	MW	10[¶]	300	3750−4600	A1m (mild)
14 Del	7974	A1 V	0.02	9 250	6	DAO	1	40	3750−4600	SB
	104	A2 V	0.03	9 150	6	DAO	3	70	3750−4600	Very faint secondary
60 Leo	4300	A1m	0.05	8 900	14	CA	1	60	3750−4453	
95 Leo	4564	A3 V	0.11	8 350	8	CA	1	30	3750−4600	SB2
32 Aqr	8410	A5m	0.23	7 600	12 (1.0:)	DAO	8	80	3750−4600	SB
ι Psc	8969	F7 V	0.51	6 250	8	DAO	3	70	3750−4600	

[*]Source: *Bright Star Catalogue* (Hoffleit 1982).
[†]T_{eff} merely corresponds to a calibration of $(B-V)$ (see text).
[§]Values in parentheses are for rotation alone (Landstreet 1998), whereas our measurements include microturbulence.
[¶]Individual exposures cover no more than half of the full span used in the project.

dispersion) and inversely to the grain size of the emulsion used. All spectra were of high resolution; the DAO instrumental profile, for instance, measured as 75 mÅ at 4500 Å from the FWHM of arc lines (in good agreement with the value of 73 mÅ determined by Booth et al. 1990 for the same equipment), is equivalent to an instrumental broadening of 2.5 km s^{-1}. Projected rotational velocities could therefore be determined empirically by broadening the arc lines to make them match the widths of the stellar lines. Our measurements agree well with those of Landstreet (1998), except for 32 Aqr. However, Landstreet segregated rotation and microturbulence whereas our values refer to the combined broadening. For 32 Aqr, he gives a microturbulence of 4.5 km s^{-1}. Each DAO spectrum covered the full extent of 850 Å (3750 − 4600 Å) used in this paper. The MW spectra were randomly centred since each included only 400 − 500 Å at higher dispersion, so were pieced together to cover the same wavelength range as the DAO spectra. Most of the CA observations were centred at shorter wavelengths than the mid-λ of the DAO spectra; as a result our spectra of ϕ Her, γ Gem and 60 Leo do not quite cover the full wavelength range used in these experiments.

The rest of this section describes the steps taken to generate accurate wavelength scales for these spectra.

3.3. Digital microphotometry

The DAO plates were traced with the DAO's modified PDS scanner (Stilburn et al. 1992). Most of the Calar Alto plates and all of the MW plates were traced with the PDS at the Royal Greenwich Observatory, Cambridge; a few were scanned at the DAO. The two machines offered a different range of set-up parameters. We used a slit-aperture of 8.5 × 350 μm at the DAO, and 10 × 200 μm at Cambridge; the output was recorded in steps of 6.01 μm at the DAO, or 5.0 μm at Cambridge. Since neither scanner provided an entrance slit that could accommodate the full height of our spectra, both had to be used in raster mode. "Clear plate" was traced as closely as possible to the stellar spectrum and with the same effective slit aperture, but with a sampling frequency of 1/20, i.e. in steps of 120.2 μm at the DAO, or 100 μm in Cambridge. Arc spectra were traced with the same step-size and slit-width as for the stellar spectra, but with the number of rasters adjusted as appropriate. The DAO scans were recorded as FITS files and were read with IRAF; the Cambridge scans were recorded in a local format. Both sets were reduced with purpose-designed software.

Direct-intensity calibration exposures consisted of (a) a sequence of contiguous strips recorded on the star plate at the DAO, (b) two sets of individually separated strips, also recorded directly, on the MW plates, or (c) a set of individually separated strips in random order observed with an auxiliary spectrograph for the Calar Alto plates. The calibration equipment and procedures at the DAO are described in detail by Richardson (1968), whilst those of MW, including the auxiliary calibration equipment also used at CA, are given by Griffin (1979). The calibration strips were

also traced in rasters, mostly at intervals of 200 Å (100 Å very occasionally), to yield the respective characteristic (H & D) curves (Hurter & Driffield 1890). The plate transmission measurements, normalized to the local, smoothed "clear plate", were converted into direct intensities by applying, at every point, the calibration relation that was nearest to it in wavelength. An extracted spectrum thus consisted of regularly-spaced intensity values recorded in the direction of the dispersion.

3.4. The problem of absolute stellar radial velocities

A cross-correlation between two observed spectra will include the difference between the actual (intrinsic) stellar velocities, together with systematic errors due to mismatch and errors stemming from processing the spectra. Clearly, the assessment of mismatch errors can only commence if the intrinsic RV difference is known and the processing errors are contained. Unfortunately, few of the wide selection of stars needed for this project have known RVs that meet our needs in terms of accuracy and precision. Early-type stars with sharp lines are often suspected of belonging to binaries, but it cannot be determined to the same degree of certainty whether those rotating more quickly are not also binary members. Sharp-lined CP stars also manifest line-blending with periods of a few days which is ascribed to spots that traverse the visible disk as the star rotates. Seeking accurate values of constant velocity for many of those stars may be impractical, even meaningless.

We circumnavigate the problem by determining a wavelength scale for each observed spectrum *within the velocity frame of the star itself*, thus making available very many more early-type stars for this project. The accuracy with which such a wavelength scale can be determined depends chiefly upon the density of the selected lines and their intrinsic widths, but also upon their intrinsic shapes. Single-lined spectroscopic binaries can thus be included in this study without requiring any knowledge of their orbital periods; even dominant primary components in double-lined systems can be used if necessary, with care. Our cross-correlation tests will therefore simply look for CCF displacements that differ from zero. But the level of accuracy achieved will depend critically upon how accurately the wavelength scales have been generated.

3.5. Deriving accurate "stellar" wavelength scales

The technique we adopt is to assign rest-wavelengths to unblended stellar lines whose relative positions are measured accurately, and to apply the grating equation to solve for the parameters describing the spectral dispersion. The calculated wavelength scale is thus anchored to the rest-wavelengths of the star. The technique was

described in the Introduction to the *Procyon Atlas* (Griffin 1979), and those authors have in fact long adopted it as routine. For stellar abundance work, where the stellar RV may not be required, it avoids the need to correct measured wavelengths for purposes of line identification. It also avoids the introduction of errors between the reference source ("arc") and the stellar spectrum; a discussion of the sources of those errors is given by Griffin (1973).

According to the grating equation, each point at wavelength λ on the focal plane obeys the relationship

$$n\lambda/d = \sin\alpha + \sin\beta, \tag{1}$$

where n is the grating order ($n = 2$ for the DAO and CA spectra described here, 3 or 4 for the MW spectra), d is the grating constant and α is the angle between the incident light and the normal to the grating. β, the angle of refraction, involves the camera focal length F and the measured position D of each point. Positions are measured relatively, so β includes a constant representing the origin of the measurements.

We measure the positions of the identified lines by cross-correlating the raw spectrum with a symmetrical, empirical profile that resembles the stellar line profiles, and select wavelengths from a homogeneous, high-quality source. The numbers of identified lines will vary widely (from ~100 downwards per span of 400 Å), depending upon the nature of the spectrum; however, it is important that they be well distributed in wavelength. Values of F and α, which are coupled, are derived iteratively by least-squares solution, and the resulting spectra are re-binned into the required step-size.

Each derivation of F and α will be affected by random errors in D and in the quoted wavelengths, by asymmetries (whether of instrumental or astrophysical origin) present in the spectrum lines, and possibly by systematic errors (e.g. thermal drifts) in the PDS; however, the latter are normally found to be negligible. Incorrect camera focus and tilt can be a significant source of instrumental asymmetry; the shapes and locations of extra- and intra-focal images differ, as is readily appreciated when examining focus tests on emission lines, and even the best focus setting will be a compromise to cope with the simultaneous existence of extra-focal asymmetries, plate-tilt errors, and irregularities in the plate-holder.

3.6. The usefulness of comparison arc spectra

The derivation of a star's radial velocity by the classical method of measuring its spectrum against a fiducial one (a laboratory spectrum) can produce low formal errors under favourable conditions. In our application of the method (see Fig. 1), F and α are first derived separately from the arc lines and from the stellar lines; the RV is then the shift required to merge the two sets and is determined iteratively, making adjustments to F and α
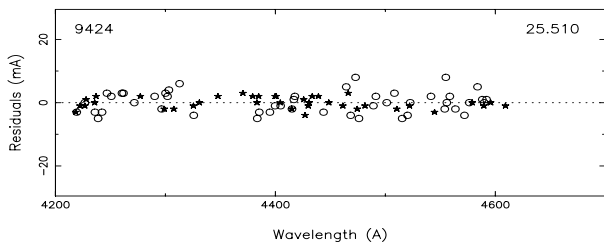
Fig. 1. Residuals, in mÅ, for arc lines (asterisks) and stellar lines (circles) on one half of a DAO exposure, after solving and correcting for the stellar radial velocity. The solution derived from arc + star combined has $\alpha = 25.510$, $F = 243.25148 \pm 0.00061$ cm, and an rms deviation of ± 3.31 mÅ for the 49 stellar lines and ± 1.69 mÅ for the 38 arc lines (0.23 and 0.12 $\mathrm{km\,s^{-1}}$, respectively, at the median wavelength). The derived topocentric radial velocity was 19.723 $\mathrm{km\,s^{-1}} \pm 0.037$ $\mathrm{km\,s^{-1}}$

so as to minimize the overall residuals. The rms deviation in Fig. 1 is 0.23 $\mathrm{km\,s^{-1}}$ at the median wavelength for the 49 stellar lines and 0.12 $\mathrm{km\,s^{-1}}$ for the 38 arc lines, with formal errors of 0.03 $\mathrm{km\,s^{-1}}$ and 0.02 $\mathrm{km\,s^{-1}}$, respectively, while the formal precision of the measured RV difference between them was 0.037 $\mathrm{km\,s^{-1}}$. However, those levels of precision are misleading, as we now show.

The method outlined in Sect. 3.5 obviates the need for a fiducial wavelength reference. Nevertheless, because arc lines are always more narrow, and usually more numerous, than stellar lines in early-type spectra, F and α for a given exposure can in principle be derived with higher precision from arc lines. We therefore applied the grating equation to the Fe-Ar arc spectra on the DAO exposures, measuring the positions of all unblended low- and medium-strength lines by cross-correlation with a matching, symmetrical emission profile, and adopting Ar I, Ar II, Fe I and Fe II wavelengths from the NIST database (http://physics.nist.gov/cgi-bin/AtData/main_asd). Measurements of the arc spectra on either side of a star spectrum were averaged. The pairs of data points (wavelength, position) constituted a set of simultaneous equations whose solution yielded least-squares values for α and F.

Figures 2a and 2b show typical optimized solutions for the separate halves of a DAO exposure; the rms scatter of the points around zero, in $\mathrm{km\,s^{-1}}$ at the median wavelength, is recorded in the caption. Lines near the extreme short- and long-wavelength ends were not used as they tend to be distorted through vignetting in the spectrograph. Lines within at least 1 cm of the plate join were also rejected; as a wet photographic emulsion dries it does so at the edges first, causing slight stretching and distortion there and producing wavelength residuals close to the plate join (positive for the short-wavelength half of an exposure, negative for the other) that are several times larger than the expected accidental errors.
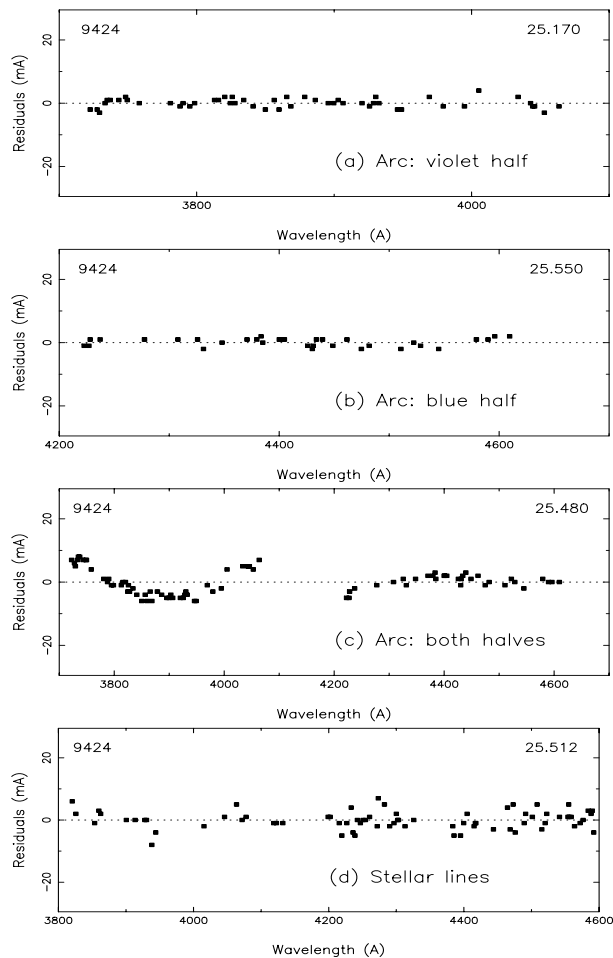

Fig. 2. Residuals, in mÅ, for arc lines **a-c)** and stellar lines **d)** on DAO plate 9424. The individual solutions give:

	α	F (cm)	S.d.* ($\mathrm{km\,s^{-1}}$)	No. of lines
(a)	25.170	242.91535 ± 0.00046	0.015	51
(b)	25.550	243.28199 ± 0.00063	0.016	33
(c)	25.480	243.19090 ± 0.00035	0.029	84
(d)	25.512	243.25267 ± 0.00036	0.020	74

*Standard error in the wavelength scale.

As the caption to Fig. 2 indicates, the two halves of the same plate do not yield the same solution, and the differences are well outside the respective error bars. Accordingly, when the two halves are brought together (Fig. 2c), the solution can only force a compromise that suits neither half as well as do the individual solutions. The two curves in Fig. 2c are actually part of the same curve, but because the measurements of line positions were not continuous across the plate join the wavelength solution has been able to introduce an arbitrary shift between the two halves in an effort to minimise the overall errors. All the arc spectra behaved in a similar fashion, apart from random errors of measurement. The same effect was

also visible (though with increased noise) in the individual arc exposures above or below the star exposure.

We have not yet found a satisfactory explanation as to why the physically separate halves of an exposure should consistently give distinctly different sets of scaling parameters (α, F). Possible causes include misalignment in the arc, image-slicer or camera (its focus or tilt), the collimation of the spectrograph, optical vignetting, errors in the figure of the camera mirror or in the plate-holder, or an error of runs in the grating. The pattern of residuals from the DAO spectra maintained a similar amplitude regardless of the epoch or the observer; it therefore seems unlikely that the cause lay in a single maladjustment (such as camera focus) over which the observer has control, though camera tilt is less industriously investigated, and spectrograph collimation is not often altered. A similar effect was also found, in a separate investigation, in arc spectra on plates from both Calar Alto and Mount Wilson. At CA the effect was less pronounced, while at MW it was similar in magnitude to that at the DAO but in the reverse sense. At the DAO and CA the grating is used almost normal to the incident beam whereas at MW it is used at a substantial angle of incidence, so indeterminacy in the grating equation is not thought to be a cause. In our investigation of the stellar spectra themselves (Sect. 3.7), where random noise was sufficiently small we found indications of the same anomaly but smaller in amplitude, and in one case of particularly sharp stellar lines it was not present at all (Fig. 2d). The formal error for the stellar lines in that example is only 1.5 times the values derived for the half-sets of arc lines in Figs. 2a or 2b. But the optimal solution of 25.512 for α differs significantly from the 25.480 derived from the arc lines (Fig. 2c); imposing one value upon the other solution gives unacceptably bowed residuals. We can summarize the situation by stating that, for stellar spectra, the systematic errors in the residuals tend to be smaller than the random errors, whereas the reverse is true for arc spectra.

We recall that we only proposed the use of arc spectra here in the expectation of improving the precision in our stellar wavelength scales. Clearly we cannot rely upon arc spectra for that purpose to the level of accuracy required, though we can estimate an uncertainty of $\sim$1.5 mÅ (0.1 km s^{-1}) arising from our *procedure* (as opposed to other internal errors, Sect. 4.2.2), with the formal error of 0.02 km s^{-1} as the lower limit. The findings have actually raised more questions than they answered, not all of which are directly relevant to the tasks set by our project, and merit a study of their own. The search for the cause(s) of the anomalous behaviour in arc spectra would benefit from studies of other wavelength regions and other spectrographs, and could make use of archived spectra. Unfortunately, few of the sharp-lined stellar spectra from CA and MW which we used in this study included suitable arc exposures.

3.7. Wavelength scales for our test spectra

We determined wavelength scales directly for the stellar spectra. Positions of identified stellar lines were measured on each exposure by cross-correlation with a matching, symmetrical absorption profile, and least-squares values for α and F were derived, as above. Stellar wavelengths were taken from the solar tables by Pierce & Breckinridge (1973), where the estimated total error (systematic + random) in the blue region is given as $\pm$ 3 mÅ. Given the experience of Sect. 3.6, we decided to treat each half of a stellar exposure independently. The solutions did not include high-order terms (i.e. no curvature of the residuals). Since many of the DAO spectra had been obtained in homogeneous series, the values of (α, F) derived for the sharp-lined stars were helpful in constraining the solutions for spectra with less sharp lines (i.e. with intrinsically higher random errors).

We attempted to optimize the wavelength solutions by considering the residuals from the same lines measured in different spectra. Some lines gave unacceptably poor residuals, either because of random errors in the stellar measurements or the solar wavelengths – many lines in A-type stars are very weak in the solar spectrum – or because of unsuspected blending, and were rejected. Lines were also rejected from individual plate solutions if the residuals were greater than 10 mÅ, and were not used at all if they proved to be bad in more than half of the samples in cases of multiple exposures. We then examined the three spectra for which we had multiple homogeneous exposures (13 of o Peg, 11 of HR 7664, 8 of 32 Aqr), and determined for each star the straight mean of the wavelengths calculated for each individual line, normalizing the means so as to eliminate an overall shift. With little variation, the adjustments to the formal wavelengths were similar in sign and size in all three stars. We then adopted these adjusted wavelengths as our new reference ones for all the spectra and repeated the wavelength solutions, extracting spectra in steps of 10 mÅ. The spectra were finally normalized in intensity by placing the continuum at 100%.

Each DAO spectrum was extracted in two intervals, $\lambda 3750 - 4150$ Å and $\lambda 4200 - 4600$ Å, conjoined with a 50-Å blank continuum; we thus avoided the troublesome plate joins, and also accommodated small differences in the precise centering of the different exposures. The CA and MW spectra were also extracted within the same overall interval, as far as the extent of each individual observation permitted.

4. Cross-correlating the spectra

4.1. General procedure

Since an RV shift is linear in log λ, we re-binned each spectrum in uniform steps of log λ, choosing a step size $\Delta(\log \lambda) = 2.3 \; 10^{-6}$ as a reasonable compromise to match both the spacing (10 mÅ) and the number of points

(mostly 85 000) in the original spectra. One bin thus corresponds to 0.75 km s^{-1}. Since mismatch shifts may depend on a great variety of factors, both astrophysical (see Sect. 2) and related to the technical details of an RV measurement (e.g. the choice of a suitable spectral "window" to be used), the first step in our strategy to study those shifts was to choose one spectrum (of high S/N ratio, to reduce random errors) as a reference template and to cross-correlate all the other spectra in turn against it. The obvious choice for this reference was the Sirius spectrum because of its high quality (see Table 1), and because its temperature is more or less at the median of the range covered by our sample. Vega, also of high quality, seemed less suitable because its lines are somewhat weaker and have unusual profiles. At a later stage we also used other spectra as a common template and investigated the mismatch shifts which occur when (as in Paper I) the temperature difference between template and object was kept to a minimum.

A cross-correlation measurement extended across 161 bins, yielding a smooth curve (CCF) whose centroid was the required RV measurement. Anticipating that the CCF might not be symmetrical (frequently it was not), we generated the mirror image of each cross-correlation and superimposed the pairs graphically, allowing the fit to be modified manually. For symmetrical CCFs the position of the centroid was judged from the central section, which was normally not more than 40 bins wide, though in cases of asymmetry we considered only the central region of that.

We recall at this point that, in the absence of spectrum mismatch, the only expected deviations of a CCF's centroid position from zero will be caused by random or systematic errors originating in the processes of observation, data reduction and shift measurement; we refer to those errors as *internal errors*, as distinct from possible bias originating elsewhere. We also remark that any shifts due to spectrum mismatch, though formally "systematic errors" in the framework of an RV measurement, are not regarded as errors *per se* in the present study.

The main results from cross-correlating the test spectra against Sirius are summarized in Fig. 3, which illustrates the dependence of the mismatch shifts on temperature. To achieve those results we followed a specific set of procedures, though only after various iterations since it was necessary first to recognise, control and as far as possible quantify the factors other than strict spectrum mismatch which could contribute their own RV shifts.

The interpretation of those results, with a discussion of the different effects of diverse kinds of spectrum mismatch, is presented in Sect. 5. In the present section we discuss the procedures adopted: the selection of spectrum "windows" of various widths and purposes (Sect. 4.1.1), and why we truncated the spectra at 95% of the continuum level (Sect. 4.1.2). We also conduct tests on subsets of spectra in order to examine the internal errors
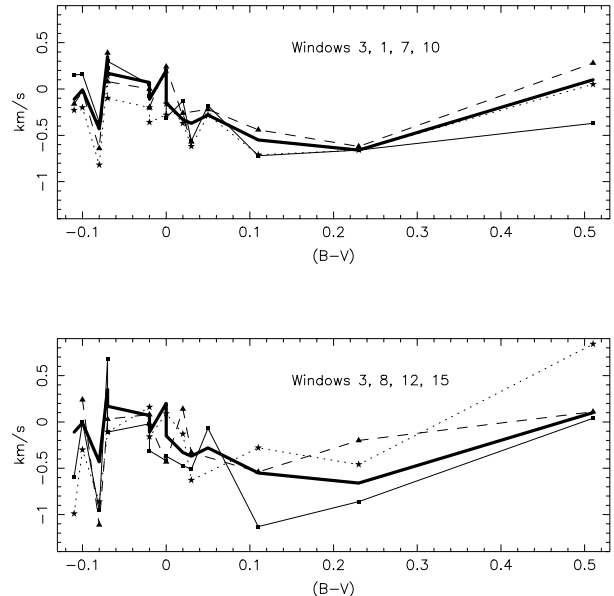

Fig. 3. Measured RV shifts, in km s^{-1}, resulting from cross-correlating test spectra against Sirius. The abscissa is the $(B - V)$ of the test star. The heavy line drawn in both panels refers to Window 3. The upper panel compares the curves derived from using Windows 1 (thin full line and squares), 7 (dotted line and asterisks) and 10 (dashed line and triangles). The lower panel compares the results from using Windows 8 (thin full line and squares), 12 (dotted line and asterisks) and 15 (dashed line and triangles)

(see Sect. 4.2), and describe other possible sources of error that might affect the results (Sect. 4.3).

4.1.1. Window selection

As in Paper I, we selected "windows" to restrict the wavelength range of the cross-correlation, though here we included only three of Paper I's windows (Nos. 16-17, 17-18 and 18-19). Somewhat in contrast to Paper I, which employed window widths all around 30 Å (except for those containing a Balmer line), we have chosen windows with a variety of widths, ranging from the total useable range of 850 Å down to only 14 Å. One purpose was to study the effects of isolating or excluding different groups of astrophysically-significant features such as the Balmer lines (Window 4), the Ca II K line (Window 5), lines of Fe I RMT 43 (Moore 1945) in Window 6 (λ 4063 Å is a temperature-dependent blend of two Fe I lines of different excitation potential), and other temperature-dependent blends, e.g. Fe II and Ti II at λ 4534 and 4549 Å (Windows 13 and 14). The wavelength limits of the windows are listed in Table 2. Care was taken to ensure that the end wavelengths occurred in continuum regions for all the spectral types considered. For that reason the first 32 Å of spectrum could not be included in Windows 1 and 4.

Table 2. Windows for the cross-correlations

no.	Start λ (Å)	End λ (Å)	Span (Å)	Comment
1	3782	4600	818	Full span
2	3811	4600	789	Balmer lines omitted
3	3811	4600	789	No Balmer lines or K line
4	3782	4127	345	Balmer lines only (5)
5	3924	3940	16	K line only
6	4038	4073	35	Fe I, RMT 43
7	4141	4292	151	All lines between Hγ & Hδ
8	4230	4265	35	sub-set of Window 7
9	4265	4282	17	sub-set of Window 7
10	4382	4600	218	Longward of Hγ
11	4406	4420	14	Prominent lines at early A
12	4500	4600	100	
13	4510	4537	27	Window 16-17 of Paper I
14	4537	4570	33	Window 17-18 of Paper I
15	4570	4600	30	Window 18-19 of Paper I
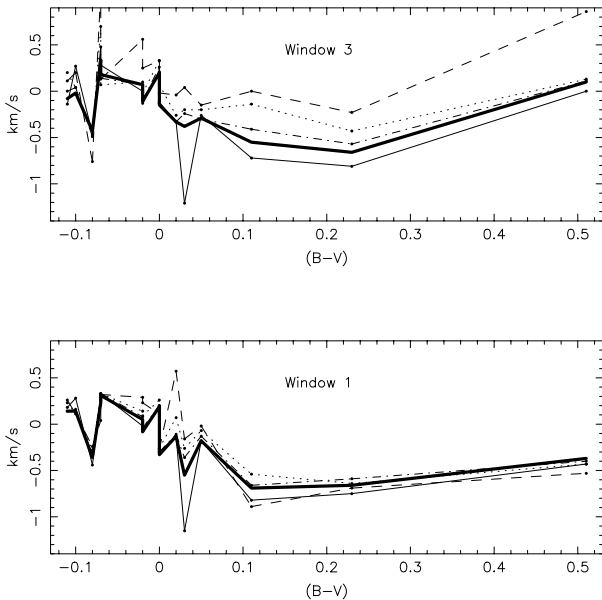
Fig. 4. RV shifts measured by cross-correlating test spectra against Sirius when the test spectra have been truncated at different percentages of the continuum. Heavy line: 95% truncation (the same heavy line as in Fig. 3). Thin line: no truncation. Other truncations represented are 90% (dot-dash line), 80% (dotted line) and 70% (dashed line)

4.1.2. Should the spectra be truncated?

We experimented with truncating the spectra at different levels below the continuum, both to gauge the effect of avoiding contamination from weak lines in a faint secondary spectrum, and also to discover whether the line cores produced a more reliable signal than did the total line profiles. Figures 4a and 4b show the results for Windows 3 and 1. Cut-offs at 90% or 95% produced almost the same results as no cut-off at all (though with one notable exception), whilst truncating the spectra below

90% induced large systematic trends. The exception was HR 104, long documented as a single-lined spectroscopic binary (Udick 1912) but in which very weak lines from its faint companion have more recently been discerned on low-noise spectra (Hill et al. 1993). The influence of its faint secondary is very evident from the large excursion in the thin line (no truncation) at $(B-V) = 0.03$, and clearly has to be avoided; the possible influence of a faint spectroscopic companion is investigated from a more general point of view in Sect. 5.5. We found that excluding the continuum tended to improve the contrast and the cleanness of a CCF. We therefore decided to truncate all the spectra at 95%, as a general compromise between including as much of the height of each feature as was reasonable whilst at the same time excluding any contribution from a secondary spectrum that might be present but scarcely visible. We note, however, that in so doing we may have biased the CCF by up to +0.2 km s^{-1}.

It is interesting that Window 1 shows relatively little variation of RV shift with cut-off level for the cooler half of the diagram, ranging from about 0.4 km s^{-1} at $(B-V) = 0.1$ to 0.2 km s^{-1} at $(B-V) = 0.5$. We attribute that apparent lack of sensitivity to the fact that Window 1 includes the Balmer lines, whose effects on the CCF are dominant and do not alter much if the cut-off level is dropped from the continuum down to 70%.

4.2. Assessment of internal errors

Our scheme for imposing a zero-velocity wavelength frame conveniently avoids external systematic errors arising from comparisons with arc spectra, but internal errors are of course inevitable. We first consider the main error sources individually and then attempt to judge their total size by comparing sub-sets of spectra of the same objects.

4.2.1. Sources of internal errors

Among the internal errors, both random and systematic contributions can be identified. Photon noise causes a truly random error on the spectra, in the sense that the errors on neighbouring pixels are not correlated (except, probably mildly, through the process of rebinning). There may also be other errors which arise randomly in the process of observation, but which vary on a scale much larger than the sampling step and could therefore be regarded as systematic, depending on the use that is made of them. For example, a non-uniform distribution of detector grains can adversely affect a line's shape and symmetry (and hence its position), the problem increasing as spectral lines are weakened for reasons associated with a star's spectral type, or (more importantly) broadened through rotation; local infelicities in the clear-plate level might have a similar effect. The level of those errors is partly reflected

in the S/N values in Table 1. We mention parenthetically that line *intensities* measured photographically are subject to errors in the calibration procedure, but those have no impact upon line *positions*; in any case, comparisons of spectra in instances of multiple exposures used in this study showed satisfactory interagreement. The random errors in the spectra propagate into the CCF (albeit at a much reduced level, which is of course the main advantage of cross-correlation) and thus cause a random error in the measured RV shift. This last increases directly with the widths of the lines and inversely with the number of lines in a window. Its magnitude is therefore related to the nature of a spectrum (hence the "phenomenological" approach announced above), and is difficult to quantify in general terms.

Unlike most centroiding algorithms, the procedure described in Sect. 4.1 does not involve any model-fitting, so we thus eliminate at least the possibility of a systematic error arising from the fact that the model to be fitted does not describe exactly the underlying function whose position one is trying to determine. Instead, however, it adds a contribution to the random error owing to the fact that the position of even a noise-free peak cannot be read back with infinite precision. Nevertheless, for a strong, symmetrical CCF the method of measuring the peak position by inverting it precludes an uncertainty of < 0.03 bins, or 0.02 km s^{-1} since the spectra are binned in steps of 0.75 km s^{-1} (10 mÅ). That uncertainty is very modest compared to the total internal errors described in Sect. 4.2.2.

Possible errors in stellar wavelength scales have been addressed in Sect. 3.6, where the systematic error in a wavelength scale was estimated to be $0.02 - 0.1$ km s^{-1}, the upper limit being judged from the way in which we were obliged to handle each spectrum reduction separately in the face of a lack of full agreement between the two halves of an exposure. We feel confident, however, that by treating each half of an exposure separately those errors were kept to a minimum – as will in fact be borne out by the small sizes of the total internal errors, at least part of which are random. Other systematic errors may arise from the process of levelling, which may be somewhat subjective when bridging the broad profile of a Balmer line or when smoothing a local irregularity in the background intensity, but are only of second-order importance here.

These systematic errors in the spectra deform the CCF, contributing an error to the measured RV shift. However, despite its undoubtedly systematic origin, this error is not necessarily to be regarded as itself systematic, i.e. it is not necessarily correlated with errors of the same origin in comparable measured RV shifts. In fact, an error in the wavelength scale does not amount to a uniform offset but is a (slowly) varying function of the wavelength, depending on several factors which are themselves random in nature (e.g. noise in the lines which were selected to define the wavelength solution) or whose distribution among the sample of stellar spectra is heterogeneous – such as the nature of an individual spectrum (chemical composition, line widths and profiles) or a tendency for a temperature-based dependence upon different solar wavelengths. Thus, an error in the wavelength scale is generally *not reproducible* (or only partly reproducible) from one spectrum to the next, even among spectra of identical objects. Likewise, an error in the function used for levelling, though systematic within a given spectrum where it has to perform a specific task, will not be identical for different spectra. So when we compare two measurements of position, the error in either can have a contribution originating from "systematic" effects but generally those contributions are not (or only weakly) correlated and may therefore be treated as contributions to the *random* error of the measurements.

The above conclusion is of course based upon the specific nature of the data we are using here and cannot be generalized to all systematic errors in any other kind of spectra. Even in the present case it has to be used with caution, because one can conceive of situations where it is not valid; for example, if spectra are cross-correlated against the same template within a window which is sufficiently narrow that an error in the wavelength scale is approximately constant over that window, an actual bias will be caused in the series of measurements. But fortunately our main conclusions do not rely upon any such special cases.

The fact that, for our present purposes, all internal-error sources can be considered as (at least largely) random allows us to describe their combined effect on the measurements by a single number, the *total internal error* (see Sect. 4.2.2). The penalty we would incur in so doing, were the assumption of randomness not justified, is an over-estimate of the error in the sense that a series of independent identical estimates would yield values distributed around a non-zero mean, with a standard deviation less than the size we shall adopt for the total internal error.

4.2.2. Estimating the total internal error

We divided the 8 spectra of 32 Aqr into two independent sub-sets, and performed the cross-correlations described at the beginning of Sect. 4.1. We also selected 4 independent pairs of 32 Aqr spectra and carried out the same tests. We repeated that procedure for the 11 spectra of HR 7664 and the 13 of *o* Peg, but in the latter case just one pair of individual spectra, selected at random, was included in the error analysis. As discussed above, the magnitude of the error is largely expected to vary inversely with the width of the window, so we examined separately the errors shown by these internal cross-correlations in two groups of windows: (a) wide to medium-wide (Windows 1 to 4, 7, 10 and 12), and (b) small, i.e. 35 Å wide or less (Windows 5, 6, 8, 9, 11, 13, 14, 15).

The results for the two A-type stars (*o* Peg and 32 Aqr) showed that the internal errors in individual spectra are near 0.06 km s^{-1} and unlikely to exceed 0.1 km s^{-1} for large windows, while for small windows they are near 0.1 km s^{-1} and unlikely to exceed 0.15 km s^{-1}. For averages of 4 or more spectra the above estimates are halved, e.g. around 0.03 km s^{-1} and not exceeding 0.05 km s^{-1} for large windows. HR 7664 (Bp) was included as an extreme case in which the density of lines is substantially lower than in the other spectra. The internal errors proved to be about twice as large for the larger windows but could rise to 3 or 4 times that amount for the smallest windows, indicating the sort of deterioration in the precision that must be expected for spectra with relatively few strong or medium-strong lines. For this star we also investigated whether the choice of cut-off level affected the internal errors, and found a small but systematic reduction in the standard deviations when a cut-off of 95% was imposed, as compared to no cut-off, thus adding a small extra weight to the decision to truncate spectra below the continuum level in order to avoid any weak secondary-star lines (Sect. 4.1.2). In general, the results of these particular tests demonstrate that the internal errors in our spectra are relatively minor and do not materially affect our main results.

4.3. Other errors

Mismatch shifts are small, so a careful assessment of all errors that might contribute is particularly important. Although the tests discussed in the previous section yield a realistic estimate of the internal errors, there are two other possible sources of systematic error – bias and sampling – to be discussed. Their effects are likely to be much smaller in cross-correlations without spectrum mismatch than in those which are the object of our study; they therefore cannot have contributed significantly to the internal error levels obtained above.

Bias may be caused by truncating the spectra slightly below their continuum levels, as mentioned in Sect. 4.1.2. For the reasons explained there we have chosen not to avoid it, but we did monitor its effects and we confirmed that it did not affect our conclusions regarding mismatch shifts. In any practical RV measurement where truncation is judged to be adviseable, this systematic error must be regarded as an independent bias; its contribution can be estimated for the spectra to hand by the sort of simple comparison illustrated in Fig. 4.

Another kind of systematic error might be anticipated to originate from interpolating the CCF position between sample steps when the CCF is asymmetrical. It would be detected as a correlation between the error in a measurement and the measurement itself. However, tests with high S/N spectra shifted over known fractions of a sample step revealed no such correlation. That result confirms that the

error originating from the measurement process is in fact random, as already assumed in Sect. 4.2.

The absence of any systematic error in our process of measurement is probably due both to the high resolution of our spectra (relaxing the demands on interpolation) and to the nature of our centroiding algorithm. The latter leaves the user in complete control of the measurement (see Sect. 4.1), so any particular asymmetry can be dealt with judiciously as the situation requires. In cases of moderate asymmetry, the procedure of fitting the central region of the CCF implied that the interfering elements were considered to be secondary and were effectively ignored (though in cases of much more severe CCF asymmetry that were encountered exceptionally in the extremes of some of our tests, the measurement was abandoned). It was on account of asymmetrical CCFs that we regarded cross-correlations involving the Vega spectrum as less reliable than most (see Sect. 5.7).

5. Interpreting the measured RV shifts

5.1. Are the Sirius results representative?

In Paper I the use of synthetic, noise-free spectra implied zero random errors, and enabled us to examine the mismatch shifts obtained for a number of quite small windows. With observed spectra, however, the presence of noise gives rise to random errors that are correlated with window size. We therefore concentrate this discussion on the RV shifts measured with the widest windows, where the random errors should be smallest, i.e. Windows 1 (everything included) and 3 (only the problematic Balmer lines and Ca II K line blocked out). We offer in Sect. 5.6 an appraisal of the other windows that were tested.

Because the wavelength scale of each observed spectrum is in its own rest-frame, the only discernible RV shift between object and template is attributable either to random and/or systematic errors, or to spectrum mismatch. Figure 3 shows one sub-set of RV shifts that were measured for the stars in our sample when (as far as we could ascertain) the total internal error was minimized. The latter is estimated as 0.15 km s^{-1} (Sect. 4.2.2), of which no more than 0.1 km s^{-1} is due to systematic errors in the wavelength scale (Sect. 3.6).

In order to interpret the residual RV shifts, and especially the curvature, shown in Fig. 3, we must first confirm the generality of the results, or discover whether any significant contribution is caused in some way by the very nature of the spectral lines in Sirius. We therefore sought to reproduce the shape of the mismatch curves in Fig. 3 by three different routes: (a) by investigating star-to-star mismatch shifts, i.e. keeping the temperature differences $\Delta T_{\rm eff}$ to a minimum, and (b) by using different stellar spectra as the template. We also examined the effects
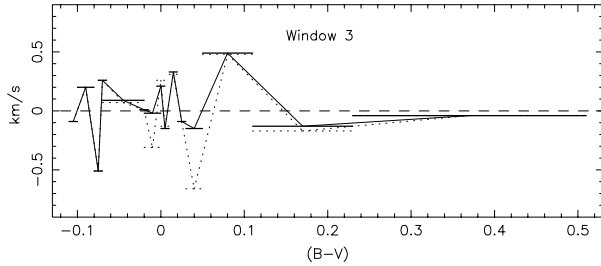
Fig. 5. RV shifts determined by cross-correlating pairs of adjacent spectra as listed in Table 1. Each horizontal bar illustrates the level of a measured shift and the $(B-V)$ interval in question. The horizontal dotted bars represent the corresponding shifts when one of each pair of spectra has (if necessary) been rotationally broadened slightly so that its line widths match those of the other star in the pair. The sets of bars have been conjoined at their midpoints to improve clarity. Note that the application of broadening tends to increase the scatter

of replacing the stellar spectra with synthetic spectra calculated for comparable values of T_{eff}, choosing as a template a model whose T_{eff} was near that of Sirius.

5.1.1. Keeping ΔT_{eff} to a minimum

We cross-correlated pairs of spectra of stars that are neighbours in Table 1, thereby minimizing ΔT_{eff}. The results, shown in Fig. 5, exhibit the pattern one would expect from a sequence of totally unrelated cross-correlations between spectra which are basically at rest with respect to one another: the mean of all the shifts is obviously very close to zero, while individual shifts are scattered around that mean. Again, the amplitude of the scatter is much larger that the expected random error so it must be due mainly to spectrum mismatch. If the curvature which is visually apparent in Fig. 3 reflects some property of the object spectra themselves, in Fig. 5 it should leave a signature in the form of a monotonically rising trend underlying the scattered shifts, but none such is apparent. We conclude therefore that a major contribution to the said curvature originates in the nature of the Sirius template.

However, if we examine the differences between successive shifts in Fig. 3 (also to be read from Table 3), we notice that the sign of those differences is mostly the same as the sign of the corresponding shifts in Fig. 5. Taking that notion a step further, we have calculated the sample correlation coefficient (CC) between the differences between successive shifts with respect to Sirius (excluding those involving Sirius itself) and the shifts in Fig. 5; its value is 0.71 and is evidence, at the 5% significance level, of a positive correlation between the two sets.
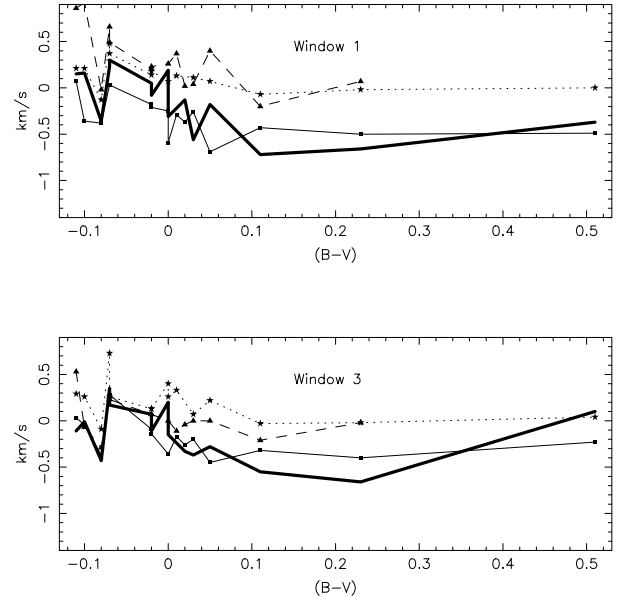

Fig. 6. Comparisons of mismatch curves measured using different templates. Thick line: Sirius template (see Fig. 3), dashed line: ι Psc (F7 V), dotted line: 14 Del (A1 V), thin line: 21 Peg (B9.5 V). The illustration has been limited to Windows 1 and 3; other windows showed similar trends but with larger scatter owing to the dominance of a few blends

5.1.2. Using other spectra as the template

The return of the curve in Fig. 3 towards zero at the coolest end of the plot suggested that the coolest star in our sample (ι Psc) might have enough spectrum lines in common with much hotter stars to constitute a useful template, notwithstanding the large ΔT_{eff} involved. We therefore selected new templates to represent the full range of T_{eff} examined: (a) ι Psc (F7 V), (b) 14 Del (A1 V) and (c) 21 Peg (B9.5 V). The results are shown in Fig. 6, where the thick lines are the same as those in Fig. 3 for Sirius. In Table 3 we list the RV shifts measured, for Window 3 only, with the four different templates.

Several features of Fig. 6 stand out:
(i) All curves define a similar relationship that is nearly flat or slightly dish-shaped with a steeper gradient for $(B-V) < 0.1$. (That commonality incidentally demonstrates a degree of objectivity in the results).
(ii) There is a marked similarity between the curves for ι Psc and 14 Del, suggesting that an F-type template can be used reliably with early A-type spectra and that one can thus build the necessary links between the zeroes of the early-type and late-type scales. The similarity in shape between the curves for ι Psc and 21 Peg suggests that a series of such links can also be extended to B-type spectra.
(iii) Again using Table 3 to calculate the difference between successive shifts, we find that the differences obtained with 14 Del as the template correlate even better with the points in Fig. 5 than do those obtained with the

Table 3. RV shifts derived by cross-correlating the programme stars against 4 different templates, using Window 3

Star	Sp. type	$B-V$	RV shifts (km s^{-1}) Template			
			Sirius	ι Psc	14 Del	21 Peg
64 Ori	B8III	−0.11	−0.11	0.53	0.29	0.03
HR 8094	B9V	−0.10	−0.01	−0.07	0.24	−0.04
HR 7664	B9p	−0.08	−0.43	−0.29	−0.09	−0.37
ϕ Her	B9p	−0.07	0.35	0.26	0.73	0.28
21 Peg	B9.5V	−0.07	0.17	0.23	0.26	
β^2 Cap	B9.5	−0.02	0.07	0.07	0.13	−0.09
o Peg	A1p	−0.02	−0.11	0.07	0.13	−0.14
Vega	A0V	0.00	0.20	−0.75	0.40	−0.36
γ Gem	A0IV	0.00	−0.15	0.00	0.26	−0.36
Sirius	A1m	0.01		−0.11	0.33	−0.17
14 Del	A1V	0.02	−0.33	−0.04		−0.26
HR 104	A2V	0.03	−0.37	0.00	0.07	−0.20
60 Leo	A1m	0.05	−0.28	0.00	0.22	−0.45
95 Leo	A3V	0.11	−0.55	−0.21	−0.03	−0.32
32 Aqr	A5m	0.23	−0.66	−0.02	−0.02	−0.40
ι Psc	F7V	0.51	0.10		0.04	−0.23

Sirius template (CC = 0.86, indicating a positive correlation at the 1% significance level). On the other hand, similar CCs for the other two templates (21 Peg and ι Psc) are 0.46 and 0.15 respectively, offering no evidence of correlation at all, possibly because of the relative extremeness of their spectral types.

(iv) There is a strong tendency for the curves for Sirius and 21 Peg to lie below the other two, and for the Sirius one to show more curvature than the other three. Other windows (not illustrated) showed the same behaviour, despite a tendency for mismatch effects caused by individual blends to dominate.

5.1.3. Tests with synthetic spectra

In order to verify our methodology, we selected models with $T_{\rm eff}$ from $7\,000 \times 500$ to $13\,000$ K (all with $\log g = 4.0$) from the set used in Paper I, and cross-correlated them against the model for $9\,000$ K (corresponding roughly to A2 V) without truncation. Because the models did not include rotation, little mismatch shift was discernible; for Window 3 the curve mimicked the upturn at the hot end of the corresponding cross-correlations between stellar spectra (e.g. Fig. 6), but with only 10% of the amplitude.

5.2. Modelling the results for the Sirius template

The tests carried out above have not reproduced the curvature that is so prominent in the mismatch relation derived with our Sirius template. In fact, the 14 Del template produced a mismatch curve that is much closer

to the flat result (zero RV shift) that was obtained with the synthetic-spectrum template. Use of the B9.5 template (21 Peg) resulted in a trend that was also flat, similar to that for 14 Del but displaced downwards from it (and from zero) by about 0.3 km s^{-1}. We also note, with some surprise, that the results seem not to depend very critically upon the magnitude of $\Delta T_{\rm eff}$.

The differences in the mismatch shifts that were generated with the Sirius and 14 Del templates were also surprising. It is important to find the reason(s), since it is only through a more general understanding of the situation that we will derive with confidence the intrinsic mismatch shifts between different stars of this spectral range. 14 Del was chosen for the test in Fig. 6 because of its close resemblance to Sirius in $(B-V)$ and spectral type (the Am peculiarity of Sirius is described as "mild"). The only pronounced dissimilarity between these two stars is their projected rotational velocities, as is visually evident from our spectra; Sirius has $v \sin i$ of about 17 km s^{-1}, while that of 14 Del is about 6 km s^{-1}. To discover whether the obvious differences between the Sirius and 14 Del curves in Fig. 6 could be an artefact of the greater projected rotation of Sirius, we created a template of 14 Del that was blurred by a rotational velocity of 20 km s^{-1} and cross-correlated the other spectra against it in the habitual fashion. The result is shown in Fig. 7, and is striking. To a first order, *all* of the excess curvature arising from using the Sirius template can be explained by the rotation of Sirius. Stellar rotation is therefore liable to cause a significant increase of the mismatch shift between two (even slightly) dissimilar spectra, *even for rotational velocities of about 20 km s^{-1}, which are very modest by A-type standards.* We amplify that statement further in the following section.

5.3. Spectrum mismatch and stellar rotation

In the case of noise-free synthetic spectra, and in the absence of other causes of spectrum mismatch, rotational mismatch has been shown to produce only neligible systematic errors (Verschueren 1991). Using numerical simulations Verschueren & David (1999) argued that, in order to keep the random error of the measurement of the CCF peak position close to its lower bound, it is nevertheless advisable to use a template whose rotational broadening matches that of the object.

For the studies of *observed* spectra in this paper we had deliberately selected sharp-lined stars with projected rotations not exceeding $20 - 25$ km s^{-1}. Most have lines sufficiently narrow that the Mg II doublet at $\lambda\,4481$ Å is partially resolved, though in Sirius and Vega that feature is a smooth blend; thus the range of $v_{\rm rot}$ in our sample is far smaller than even the individual velocity steps (50 km s^{-1}) employed by the two papers cited above. Nevertheless, in view of the high resolution of our spectra we supposed initially that we might decrease the error in the CCF position
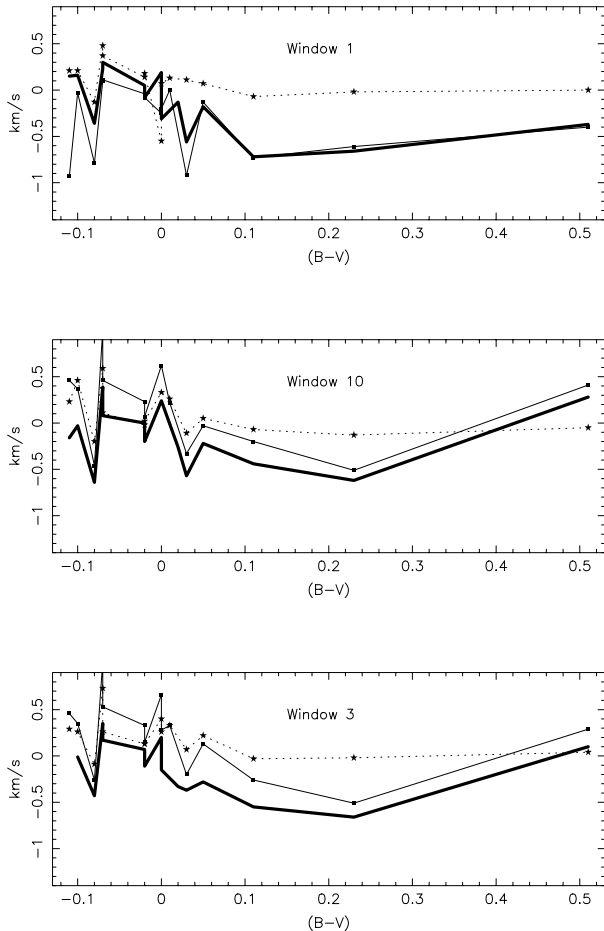
Fig. 7. Reproducing the Sirius mismatch curve. The heavy line is the curve for Sirius, while the dotted line represents the curve for 14 Del (see Fig. 6). The thin line shows the results obtained when 14 Del is spun by a rotational velocity of 20 km s^{-1}. In all three windows illustrated here, and in the top one in particular, our model of a moderately rotating A1 star reproduces closely both the curvature and the details of the Sirius curve

Fig. 8. RV shifts measured by cross-correlating test spectra against **a)** Sirius and **b)** 14 Del, when the template has been rotationally broadened up to 40 km s^{-1} in steps of 10 km s^{-1}. The heavy line in **a)** is the same as that in Fig. 3, while the heavy line in **b)** is the same as the dotted line in Fig. 7. Thin line: broadened by 10 km s^{-1} (scarcely distinguishable from the thick line); dot-dashed line: 20 km s^{-1}; dotted line: 30 km s^{-1}; dashed line: 40 km s^{-1}. These plots illustrate the results obtained for Window 3; the other windows yielded results that were qualitatively similar

by making object and template spectra match in apparent rotational velocity. However, in the case of observed spectra that premise seems to have been at least partly ill-founded, as was adumbrated by Fig. 5: the dotted lines there indicate the effects of applying a small amount (≤ 15 km s^{-1}) of rotational broadening to one member of each pair of spectra prior to cross-correlation in order to improve the visual fit. The overall result of almost zero trend is the same in both cases, but the scatter has been made worse – i.e. the mismatch shifts have increased – by applying the broadening even though the line profiles then *looked* to be more similar.

We went on to test the generality of the above results by imposing different amounts of rotational broadening upon a series of cross-correlations that used first Sirius and then 14 Del as the template. In each case we broadened the template from 10 to 40 km s^{-1} in steps of

10 km s^{-1}, and worked with Windows 1, 3 and 7. We show in Fig. 8 the results obtained (for Window 3) with the two templates: Sirius (Fig. 8a) and 14 Del (Fig. 8b). From there we draw the conclusion that any tinkering with the natural line-widths of the template, particularly in cases of very narrow lines, is liable to increase the mismatch shift.

In view of the finding that even very slight differences in spectral structure or line shapes between object and template are liable (depending on their nature and on the rotational velocities involved) to cause a systematic RV error that is well above the expected level of the random error, we can now understand why the theoretical studies did not predict this result: the conclusions of Verschueren & David (1999) were based on an investigation of synthetic spectra in which object and template were intrinsically identical.

In concluding this discussion on the effects of rotational broadening, we recall that the purpose of this series of papers is to specify a set of conditions, or limits to a general procedure, for measuring radial velocities in hot stars to a high precision and accuracy, and that one likely application will involve numerous, real-time measurements of stars in clusters for statistical analyses. An efficient system must avoid the need to determine precisely the projected rotational velocity of each individual star in order to select the best matching template. Even though the

question regarding the possible reduction in accuracy due to a difference in rotation is unanswered in the case of non-identical spectra – and is likely to remain so until there is a centroiding algorithm for an asymmetrical CCF peak which can be shown to keep the random error close to its lower bound (see Verschueren & David 1999) – one must bear in mind the risk of severely decreasing the accuracy by increasing the rotation (whether artificially or through selection) in order to match the line widths of template and object. At least for spectra of a quality comparable to ours (high but not atypical S/N ratio and resolution) it has been shown (Figs. 5, 7 and 8) that rotational matching is not only unnecessary but actually harmful to the final quality of an RV measurement.

Our conclusions (Sect. 5.7) regarding the overall magnitude and sign of mismatch shifts for observed spectra are therefore based on the use of the spectrum of 14 Del, not Sirius, as the template.

5.4. How critical is the spectral type of the template?

In Fig. 9 we have repeated the series of cross-correlations performed earlier (see Fig. 3) but using 14 Del as the template. Because the results for Vega do not assist in clarifying any general trends, they have been omitted. In the bottom panel the mismatch curve has been "tidied up" by omitting the spectra of the chemically-peculiar B stars as well, for reasons that are amplified in Sect. 5.7. The deviation shown there is less than 0.1 km s^{-1} between spectral types mid-F to A3 or A2, but rises fairly abruptly to about 0.3 km s^{-1} for spectral types A0 − B9. We note parenthetically that a spectral-type sub-class is equivalent to a somewhat larger $\Delta T_{\rm eff}$ at late B than at mid A, so the trend with increasing $T_{\rm eff}$ is actually less abrupt than is depicted.

For stars of types ∼A3 and cooler, *including those classified as Am*, an F-type template appears to suffice for measuring RVs to a high accuracy (see Fig. 6), whereas for very early-A and late-B types a positive error of $0.2 − 0.4$ km s^{-1} may be incurred if an F-type template is used, and (more importantly) the accuracy achieved will depend fairly critically upon spectral peculiarity. It is therefore adviseable to establish for the hotter stars a linked sequence of templates for different spectral peculiarities.

We tested the validity of the above statements by replacing the 14 Del template with a synthetic solar-abundance spectrum calculated for $T_{\rm eff} = 9\,000$, $\log g = 4.0$ (i.e. no more than two subclasses removed from the spectrum of 14 Del), and broadened by a rotational velocity of 8 km s^{-1}. Cross-correlations were performed as for Fig. 9, for Windows 1, 3, and 7. In Fig. 10 we compare the results obtained with the synthetic and the 14 Del templates. The closeness of the comparison confirms the objectivity of all the results derived with the 14 Del template. Since the 14 Del results resemble those for templates
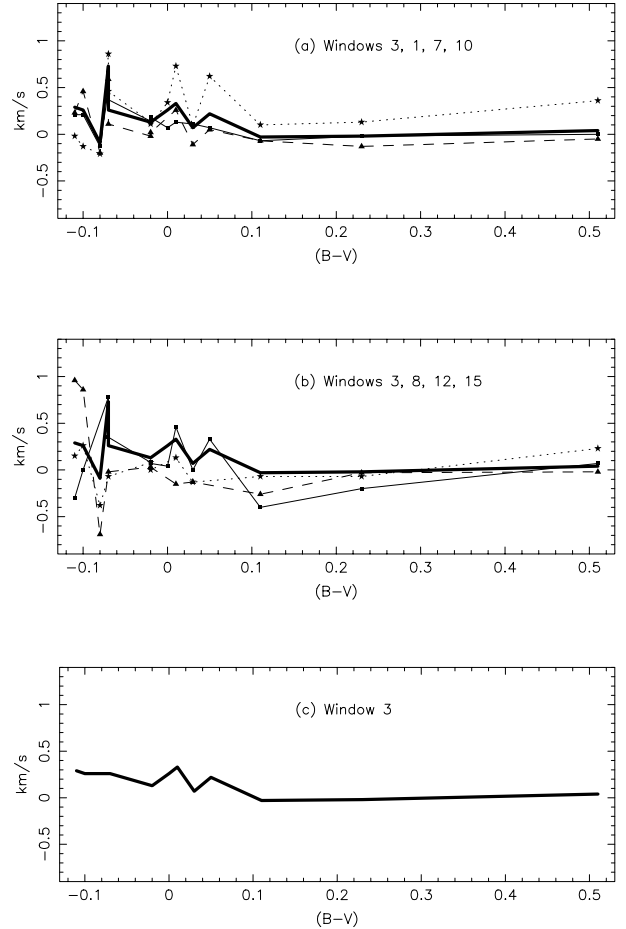

Fig. 9. The results of cross-correlating the spectra against that of 14 Del, for different windows (cf. Fig. 3). The heavy line drawn in the top two panels is that for Window 3. Panel **a)** includes the curves derived from using Windows 1 (thin full line and squares), 7 (dotted line and asterisks) and 10 (dashed line and triangles). Panel **b)** shows the results from using Windows 8 (thin full line and squares), 12 (dotted line and asterisks) and 15 (dashed line and triangles). Results for Vega have been omitted. Panel **c)** demonstrates how the scatter is reduced when the CP stars are also omitted (for reasons, see text), and enables the size of the scatter from those sources to be appreciated

at both extremes of the range, we infer that the precise spectral type of the template is not critical at all. When measuring the RVs of unknown programme stars, therefore, a guide as to their approximate spectral types would be helpful, but it is not necessary to classify the stars beforehand in any great detail.

A comparison of Figs. 5 and 9 clearly shows that the mismatch shifts between spectra which are closely adjacent in spectral type are dominated by the effects of individual differences other than those associated with a difference in $T_{\rm eff}$. A procedure that is based primarily upon the criterion that the spectral types of the objects match as closely as possible a template from a grid of MK standards alone is therefore ineffective, but will be more
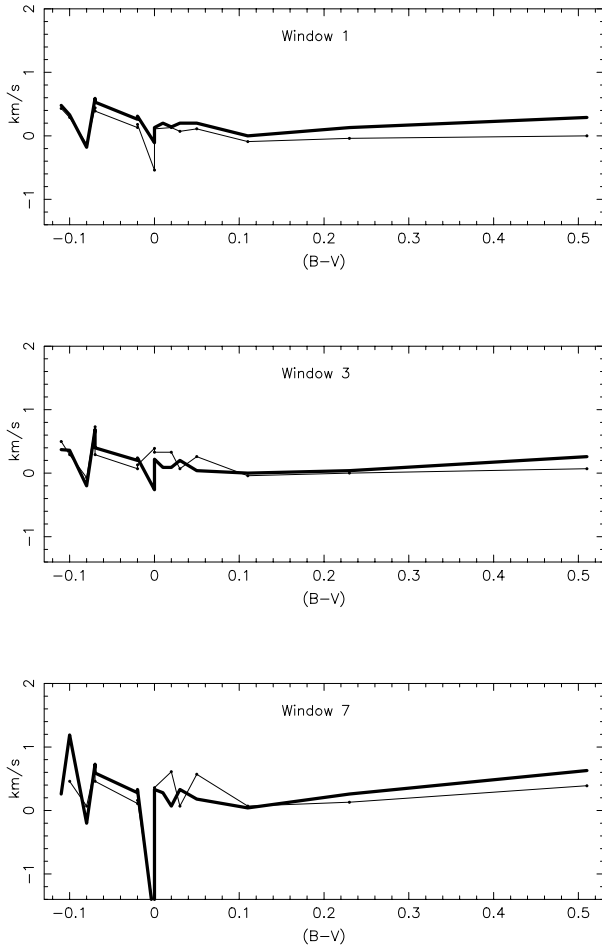
Window 1

Window 3

Window 7

Fig. 10. Comparison of stellar and synthetic-spectrum templates for three different windows. The thick line depicts the results obtained by cross-correlating the test spectra against a synthetic noise-free spectrum calculated from a solar-abundance model with $T_{\rm eff} = 9\,000$ K, $\log g = 4.0$; the thin line refers to the results for the 14 Del template

rewarding if the grid is rich enough to include a diversity of spectral peculiarities (and provided that the $v \sin i$ of all templates is sufficiently low). Since mismatch in intrinsic line profiles can give rise to larger RV shifts than does mismatch in spectral type, we conclude that – at least for the low rotational velocities represented by our sample – narrowness of line profiles should be regarded as a more important criterion in the choice of template than a close match in spectral type.

5.5. Unsuspected binary membership

HR 104 has a faint early-type companion (Hill et al. 1993). In Fig. 4 the large deviation of the thin line (no truncation) at $(B - V) = 0.03$ corresponding to HR 104 illustrates the strong disturbance to the CCF centroid that can be caused by even a faint companion spectrum if its velocity separation lies within a particular range. In order
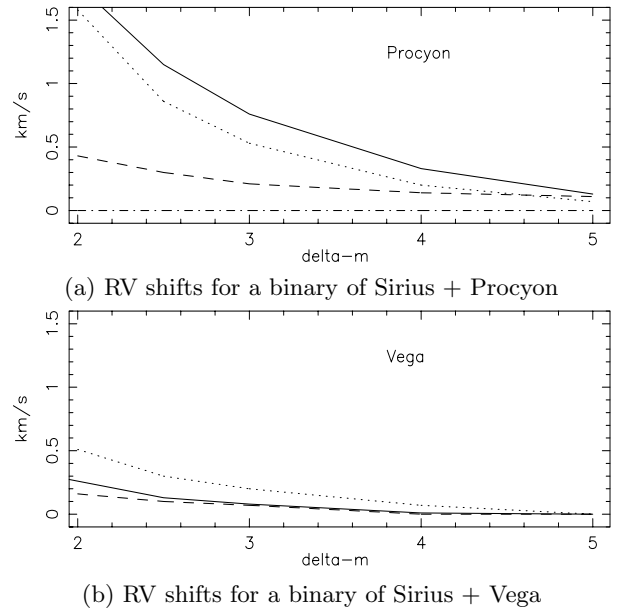
(a) RV shifts for a binary of Sirius + Procyon

(b) RV shifts for a binary of Sirius + Vega

Fig. 11. The influence of a faint companion upon the CCF (Window 3). An artificial binary was generated by adulterating the spectrum of Sirius with the spectrum of Procyon (upper plot), reduced by factors delta-m and displaced by 0.1 Å (full line), 0.3 Å (dotted line), 0.4 Å (dot-dashed line) and 0.5 Å (dashed line), respectively. The "binary" was then cross-correlated against an independent spectrum of Sirius. The results for Window 1 gave slightly larger, but generally very similar, RV displacements. The lower panel shows the results of a similar test using Vega instead of Procyon as the secondary. (The model with 0.4 Å separation has been omitted for clarity)

to examine more rigorously the conditions under which secondary spectra can or cannot be tolerated, we created two fake binary spectra. Each included a primary formed from one of two sub-sets of Sirius spectra; for the secondary, one binary incorporated the spectrum of the F5 IV-V dwarf Procyon (Griffin 1979), while the other included the spectrum of Vega (A0 V). A grid of each type of binary was then generated, in which the secondary was reduced in magnitude relative to the primary by 7 values between $\Delta m = 1$ and 5, and separated from it in RV by values ranging from 0 to 0.5 Å. Each resulting "binary" was cross-correlated with the other subset of Sirius spectra. The results for Window 3 are illustrated in Figs. 11a and 11b. Figure 12 depicts in 3-D the effect of the Sirius-Procyon binary.

These tests illustrate the non-negligible effects of even a faint ($\Delta m > 4$) secondary, and can be explained by considering the characteristics of the spectra forming the secondary in the fake binaries.

In our Procyon spectra the lines around $\lambda\,4500$ Å have a FWHM of about 0.18 Å, and half-widths at the continuum of 0.25 to 0.3 Å; in our Sirius spectra the lines have a typical FWHM of about 0.375 Å. At zero RV separation between primary and secondary there is of course no
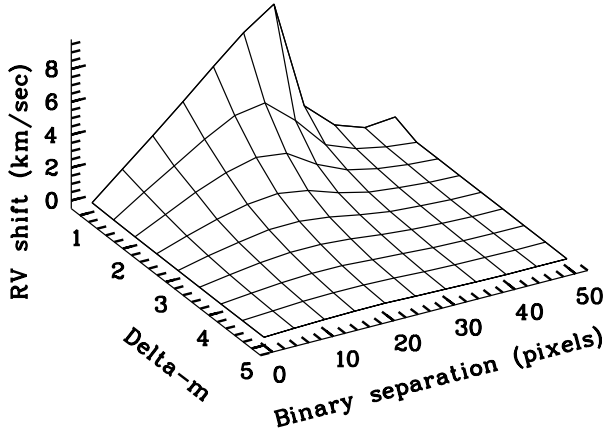
Fig. 12. 3-D description of the influence of the "Procyon" secondary in the fake binary. The maximum influence of this fairly narrow-lined secondary occurs near a separation of 30 pixels (0.3 Å). Beyond about 0.4 Å separation the secondary would scarcely affect the cross-correlation, however small the difference in magnitude, delta-m

disturbing influence upon the measured RV of the primary, but as a separation begins to grow it causes line asymmetries that deteriorate rapidly, giving rise to mismatch shifts that reach a maximum when the flanks of the secondary's lines reach just to the centre of the primary's lines (Figs. 11a and 12). Beyond that point, as the separation continues to increase the primary's contributions to the blends are less contaminated with the secondary's lines, so the mismatch shift decreases. At 0.5 Å separation enough of the cores of the primary's line-profiles are unaffected by the blending secondary that the mismatch shift falls to zero even with Δm as small as 2, and the binary can be treated as a single-lined star.

The crucial factor is therefore the width of the lines in the secondary spectrum. In Vega the FWHM was measured on our spectra to be 0.55 Å, which explains why the disturbing influence of that secondary (Fig. 11b) persists when the binary is separated by 50 pixels (0.5 Å) even though the lines in Vega are weaker than those of Procyon and their overall influence is correspondingly smaller.

We conclude that a secondary spectrum can distort a measured CCF even if the companion star is too faint to be detected spectroscopically, and even if its temperature is fairly dissimilar from that of the primary; Sirius and Procyon are about 3 000 K apart. The key factor seems to be not so much the actual temperature difference, as whether or not the secondary spectrum contains enough of the primary's spectral lines to produce a CCF signal from a template that matches the primary spectrum.

5.6. The usefulness of different windows

The windows defined in Table 2 were selected so as to include specific regions or groups of lines. It was expected that Windows 6 and 11 would only be suitable for a rather restricted range of spectral type. Thus Window 6, which contains the strong lines of Fe I RMT 43, should have worked well for the cooler test stars but not the hotter ones, though in practice those Fe I lines are themselves asymmetrical and proved unsatisfactory for all types. Window 4, which isolates the Balmer lines, gave (not unexpectedly) broad CCFs and ragged results, and was only tried for contrast; it was not employed in any of the tests to measure RV shifts or errors. An additional window to include the Si I lines near λ 3850 Å was also tried, but was abandoned because that region is contaminated by other features in all but the hottest stars.

In general, the smaller the window the smaller the number of lines (i.e. signal), so the larger the random errors in the CCF. All of our observed spectra contain internal noise, though to differing degrees, and our experiments proved repeatedly that the tests decribed in Sect. 4 were best carried out with very wide span (Window 3), with supporting evidence where possible from Window 1 and subsets of Window 3 (chiefly Windows 7, 10 and 12). Window 12, which is a subset of Window 10, also tended to give results that were consistent (within a tolerance of 0.2 km s^{-1}) with those from Windows 1, 3 and 7, as did one of its sub-divisions (Window 15), though such a narrow window is prone to increased random errors. The other windows either contained features that tended to mask the underlying trends that we were measuring, or contained too few lines for robust results.

By examining the differential behaviour of the windows we were able to identify some of the blends that cause problems. Thus, while the behaviour of Window 12 was generally good, and that of Window 15 was also acceptable for the most part, the two other subsets, Windows 13 and 14, were noticeably bad. Here our conclusions differ slightly from those of Paper I, which found that its Windows 16-17, 17-18 and 18-19 (our Windows 13, 14 and 15, respectively) all returned low shifts for low $v_{\rm rot}$. The problems with 13 and 14 stem largely from the strong Fe II–Ti II blends at $\lambda\lambda$ 4534 and 4549 Å; both are somewhat temperature-dependent, the lower exciation potentials of the Fe II lines being roughly twice those of the Ti II lines. The blend at λ 4534 Å, a very unequal juxtaposition of two lines, is fully resolved when rotation is absent, whilst the feature at λ 4549 Å is a close blend of two fairly comparable lines of Fe II and Ti II plus a more distant line, and only the latter is fully resolved for zero rotation. Even though the amounts of rotational blurring present in many of our spectra are small, they are nevertheless sufficient to cause different mismatch shifts in the observed spectra of the individual stars when
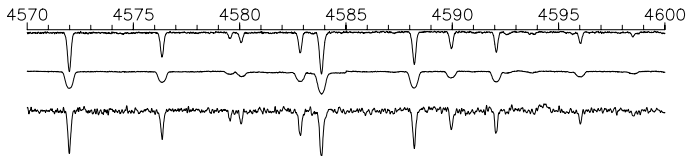
Fig. 13. Spectra of *o* Peg, A1p (top), Sirius, A1m (centre) and 14 Del, A1 V (bottom) in the region defining Window 15. The strongest lines are given (NIST database; Moore 1945) as:

λ	Identity	lower E.P.	λ	Identity	lower E.P.
4571.968	Ti II 82	1.56	4588.199	Cr II 44	4.05
4576.340	Fe II 38	2.83	4589.958	Ti II 50	1.23
4582.835	Fe II 37	2.83	4592.049	Cr II 44	4.06
4583.837	Fe II 38	2.79	4596.060	Fe I 820	3.59

the components of the blends overlap by different amounts (see Sect. 5.5).

Window 12 also contains several lines of Cr II which are enhanced in the Bp stars; Cr II lines mostly occur in Window 15, but as they are not intrinsically blended there they do not give rise to a mismatch shift. Figure 13 illustrates the lines in Window 15 in different stars at about 9 500 K. We note parenthetically that Window 15 occurs at the redward limit of our spectra where the signal was probably somewhat degraded, and unevenly so among the sample; in Sect. 6 we propose that further studies based on this region, with correctly optimized observations, should be particularly rewarding.

5.7. General conclusions

The overall results of this paper, now depicted in Fig. 9, are really quite surprising. Our cross-correlations sample a wide range of temperature ($6\,500 < T < 12\,500$), with the spectral type of the template (A1) near the median value. Enormous visible changes take place in spectral-line intensities across that range, and we would suspect that few lines were common *and sufficiently unblended* throughout. Yet it would appear that enough good-quality lines do persist between those two extremes to provide a basis for meaningful cross-correlation.

Our tests have also shown that large mismatch shifts can occur between any given pair of stars, whereas when one template is used to measure a range of spectral types a fairly smooth relationship is found, especially if extremes of spectral peculiarities and deviating line shapes are not included. We found moreover that the presence of natural broadening in the template, even as little as about 15 or 20 km s^{-1}, gives rise to a trend in RV shifts that demonstrates how rotation can aggravate the effects of spectral-type mismatch, and in addition we showed that any attempt to effect rotational matching by artificially broadening either object or template can seriously exacerbate existing slight differences in intrinsic shapes of lines

and blends, and can magnify an RV error that need not be apparent if the spectra are cross-correlated in the natural state.

The use of real spectra for these experiments has thus provided some interesting and decisive results that complement the theoretical studies, especially since we could differentiate visually between profiles broadened by stellar rotation, and profiles that are broadened by a star's characteristic surface velocity fields, or "microturbulence". The scope of the conclusions has however been limited by the S/N ratio of the observations and by the number and variety of stars in the sample. The need for high resolution in these tests has also been affirmed, particularly from our experiences with the spectra of Sirius and Vega; with coarser sampling it might not have become apparent that such modest rotational broadening does have an appreciable effect at the level of accuracy for which we are aiming, nor that line profiles could be so strikingly non-Gaussian.

The spectrum mismatch shifts depicted by the heavy line in Fig. 9 occur very largely because line blends in stellar spectra are composed of features whose relative strengths differ, principally through $T_{\rm eff}$, $\log g$ or chemical composition. Rotational broadening, whether present in the object or the template or both, will clearly tend to exacerbate that situation. Were all the lines in a stellar spectrum sufficiently isolated, none of those errors would arise. Our selection of different windows helped to identify some of the more prominent lines or blends e.g. of Fe II and Ti II at λ 4534 and 4549 Å, which are responsible for the observed mismatch shifts.

Where the dominant factor in spectrum mismatch is the difference in temperature and not chemical peculiarity, we have been able to confirm, for all but the hottest samples, the magnitude of the mismatch shifts (ΔRV $\approx$ 0.05 km s^{-1}) derived in Paper I for synthetic, noise-free solar-abundance spectra. However, inasmuch as mismatch shifts are also caused by intrinsic differences between spectra of similar $T_{\rm eff}$ but different chemical composition, the results of the present paper complement those of Paper I. For reasons already given, our sample contained several spectroscopically "abnormal" stars, there being little actual choice of "normality" owing to our insistence upon the sample being restricted to narrow-lined spectra. (The description "normal" has confusing connotations for B and A types, where the seemingly high frequency and disparity of chemical peculiarities, together with a possible bias through observational selection and high binary incidence (Ramella et al. 1989), calls into question the definition of a norm). We have shown that spectral peculiarities among stars of types late B to mid A are more deleterious in causing RV shifts than are differences in temperature between spectral sub-classes. However, since the occurrence of a foreign feature in the test spectrum close to a line that is common to both test and template is random, albeit shared to some extent by stars showing generically

the same peculiarity, chemical abnormalities chiefly cause scatter on the mismatch curve.

To identify the effects of spectral-type mismatch (to within the noise limitations of our data), we eliminated from Fig. 9 the 4 stars classified as CP (HR 7664, ϕ Her, β^2 Cap and o Peg) – see Fig. 9c. We also eliminated Vega because its lines have profiles that appear sufficiently unusual (see Sect. 2.2) to cause particularly deleterious mismatch, but retained the metallic-lined stars since their abundance peculiarities are chiefly represented by an *overall* strengthening of metallic lines. The curve in Fig. 9c has much less noise than those in Figs. 9a and b, and indicates how much of the small-scale scatter in the upper parts of those and similar figures is attributable to chemical peculiarities. Figure 5, on the other hand, is not substantially changed by eliminating the CP stars.

Similarly to what we found in Paper I for spectra with high rotational velocities, the results from the reduced sample suggest that for slow rotators too the RV displacements caused by spectrum mismatch are not as random as might be supposed intuitively (or as Fig. 5 might be thought to indicate). Even across a span of more than 800 Å the mismatch shift for the hotter stars is systematic. The tendency of mismatch curves to turn upwards towards the earlier types (see Fig. 9c) reflects a correlation between the temperature of the hotter objects and the mismatch shift, if a fixed template is used. We note that Morse et al. (1991) also found the same positive correlation of shift with ΔT_{eff} for $T > 9\,000$ (the lower limit of their study). We have also shown that the gradient towards decreasing $(B - V)$ is independent of the spectral type of the template (Fig. 6).

There is a general trend towards smaller mismatch shifts at the cooler end of the sample even when the template's lines are broader than those of the test spectra (Figs. 3, 8). While it is true that the cool stars in our sample do not include such striking chemical peculiarities as occur among the hot ones, the chief reason for that trend is (we suggest) an increasing tendency for mismatch shifts arising from individual blends or groups of blends to cancel statistically with increasing lateness of type as the density of lines grows. Microturbulence may also tend to increase with cooler A types (Landstreet 1998), slightly counteracting the benefits of an increasing line density; however, its links to the structure of the convective movements in a stellar atmosphere imply a dependence upon spectrum peculiarities and hence wide individual deviations from the norm, and it will require a much larger sample of spectra than ours to support a quantitative differentiation between its effects. At present we can simply give the opinion that, in most applications, the total RV error will best be contained by choosing a template with the narrowest possible lines, and disregarding any "rotational mismatch" between object and template.

We have shown that it will be possible to measure RVs to an accuracy considerably better than 1 km s^{-1} for slowly rotating stars in the temperature range examined, provided certain criteria are met in the selection of the template spectrum. In view of the large range of spectral idiosyncrasies that occur beween mid-B and early-A types, a choice of stellar templates is likely to prove more reliable than a grid of synthetic spectra which is not able to include either the diverse spectral peculiarities of CP stars or a good detailed representation of stellar velocity fields. In choosing a stellar template to minimize systematic mismatch shifts, the principal criterion is for as little rotation as possible. The other criteria specify that the spectra need to be of sufficiently high S/N ratio that random errors are contained, and (obviously) as free as possible themselves from internal systematic errors (e.g. in wavelength scales). For many applications the cross-correlation should use a window of maximum width. Figure 9 shows that the mismatch curve may exhibit considerably more scatter when a small-span window is used in cross-correlating real spectra, though in the next section we comment on the potential of using a small window in the case when it does not contain any harmful blends and when random errors are controlled by employing very high S/N. We must however point out that the above results have been reached through studies of quiescent dwarf stars, and may therefore only be applicable to those and similar stars.

6. Applications of the results, and concluding comments

Considerations of the noise levels even in ostensibly high S/N spectra lead us to conclude that cross-correlations using observed spectra should involve as many metallic lines as possible. That of course reflects the situation with cool stars and CORAVEL instruments, in which one seeks to increase the precision of the CCF peak by designing a template that samples a great many lines simultaneously. One possible feature in the design of high-accuracy RV measurements of early-type stars is therefore a very wide template spectrum in order to maximize the signal from unblended lines and thus outweigh the systematic errors arising from spectrum mismatch, at least in the case of stars with low $v \sin i$.

However, we have also found a strong indication that lines in the neighbourhood of $\lambda\,4570-4600$ Å (see Fig. 13) are sufficiently blend-free for slowly-rotating stars that that region alone can yield RV results with very little contamination from spectrum mismatch. The 5 lines of Ti II and Fe II between $\lambda\lambda\,4500-4524$ Å, with which Fekel (1999) has achieved consistent RV measurements for B and A stars, holds out similar promise. Another route to achieving the goal of rapid, accurate RV measurements for an assortment of early-type stars might therefore be to observe a narrow window around those wavelengths with particularly high S/N ratios. Since the causes of spectrum mismatch are only important if lines are blended,

a window that is largely devoid of blends should work satisfactorily for a wide range of spectral types, as the present study has demonstrated, and an accurate foreknowledge of the spectral types or colours of the programme stars should not be necessary.

The only spectrum we felt obliged to eliminate at any stage was that of Vega, the one-time archetypal standard A0 V, on account of its slightly abnormal line profiles. It is not inconceivable that part of the problem encountered with the spectrum of Vega was caused by systematic errors in the wavelength scales of the individual spectra brought about by the difficulty of measuring the centroids of non-Gaussian profiles. We must add, however, that although our experience with the spectrum of Vega in this context may appear to have been negative, the message behind those results is in fact strongly positive, and makes a clear case for the use of the highest possible spectral resolution in conducting tests of this nature. It is also a warning of one type of *astrophysical* limitation to the objectives of this project.

In this paper we have not investigated the effects of spectrum mismatch for spectra that are rotating more than about 25 km s^{-1}. Our method of determining the wavelength scale "internally" would require particularly high S/N observations if large systematic errors in the wavelength scales of more rapidly rotating stars are to be avoided. Tests on a high-resolution spectrum of the A2m dwarf ϵ Ser, whose $v \sin i$ we measured as 35 km s^{-1}, demonstrated that difficulty: even in the case of this relatively rich spectrum, the scatter in the RV shifts was large enough to obliterate the delicate trend of spectral-type mismatch shifts that we now know to exist from the above studies on very narrow-lined stars. This does not mean however that rotationally-broadened spectra can be handled any better by the conventional methods of determining wavelength scales from arc spectra, whether with a classical or an echelle grating, since the absolute velocity of the star still has to be determined. It merely suggests that high S/N will be of paramount importance for measuring the spectra of rotating stars and that even so it will be very difficult to achieve absolute RV measurements for such stars with a precision and accuracy that approaches what we have been able to demonstrate in this paper.

We have not mentioned the possibility of designing a physical mask to measure the RVs of these hot stars. There is already a wide acceptance that the diverse and relatively impoverished nature typical of hot-star spectra will immediately prove such a method to be impracticable. The flexibility offered by the use of numerical templates is surely essential.

We therefore conclude with twin recommendations for the pursuit of high-accuracy RVs for early-type stars: *either* a very wide window *or* a very narrow one, depending upon the available observational material and the immediate goals of the investigation. If the objective is to study conditions of spectrum mismatch among stars of very

different rotational broadening (an aspect which this paper did not address), a wide window will probably be the better choice for that purpose in consideration of reducing random errors, and of blocking out the worst regions in cases of rapid rotation (see Paper I). Archived spectra would continue to be prime sources for such a study, ensuring a large amount of already-available observational material that needs no expenditure of observing resources.

If, on the other hand, the goal is to establish a small number of very high-quality spectra to serve as templates for as wide a range of spectral *types* as possible, a narrow window such as Window 15 is likely to serve best. As in the present study, the wavelength scales of the spectra should be determined in their intrinsic velocity frames. A good-quality CCD plus classical grating should be an ideal combination, and we hope to make such an investigation the topic of another paper in this series. Since it will not be so easy to establish accurate results for highly rotating stars by the use of a narrow window, both approaches need to be developed in parallel in order to achieve the overall goal of measuring accurate RVs for early-type stars.

References

Baranne A., Mayor M., Poncet J.L., 1979, Vistas Astron. 23, 279

Baranne A., Mayor M., Queloz D., et al., 1996, A&A 119, 373

Booth A.J., Blackwell D.E., Fletcher J.M., 1990, Pub. Dom. Astr. Obs. 18, No. 1

Dravins D., 1985, in: Davis Philip A.G., Latham D.W. (eds.), IAU Colloq. 88, Stellar Radial Velocities. L. Davis Press, N.Y., p. 311

Dravins D., 1999, in: Hearnshaw J.B., Scarfe C.D. (eds.), IAU Colloq. 170, Precise Stellar Radial Velocities, ASP Conf. Ser. 185, 268

Fekel F.C., 1999, in: Hearnshaw J.B., Scarfe C.D. (eds.), IAU Colloq. 170, Precise Stellar Radial Velocities, ASP Conf. Ser. 185, 378

Fletcher J.M., Harris H.C., McClure R.D., Scarfe C.D., 1982, PASP 94, 1017

Flower P.J., 1996, ApJ 469, 355

Griffin R.F., 1967, ApJ 148, 465

Griffin R.F., 1968, A Photometric Atlas of the Spectrum of Arcturus. Cambridge Philosophical Society

Griffin R. & R., 1973, MNRAS 163, 243

Griffin R. & R., 1979, A Photometric Atlas of the Spectrum of Procyon, R. & R. Griffin

Griffin R. & R., 1988, Observatory 108, 114

Griffin R.F, Gunn J.E., 1974, ApJ 191, 545

Gulliver A.F., Adelman S.J., Cowley C.R., Fletcher J.M., 1991, ApJ 380, 223

Hill G., Adelman S.J., Guilliver A.F., 1993, PASP 105, 748

Hoffleit D.M., 1982, Bright Star Catalogue, Yale Univ. Obs., New Haven, Conn.

Hurter F., Driffield V.C., 1890, J. Soc. Chem. Ind. 9, 455

Jaschek C., Gómez A.E., 1998, A&A 330, 619

Landstreet J.D., 1998, A&A 338, 1041

Latham D.W., Stefanik R.P., 1992, Trans. IAU, Vol. XXIB, p. 269

Moore C.E., 1945, A Revised Multiplet Table of Astrophysics Interest, Contr. Princeton Obs., No. 20

Morse J.A., Mathieu R.D., Levine S., 1991, AJ 101, 1495

Pierce A.K., Breckinridge J.B., 1973, Contr. Kitt Peak Nat. Obs., No. 559

Ramella M., Gerbaldi M., Faraggiana R., Böhm C., 1989, A&A 209, 233

Richardson E.H., 1968, J. Roy. Astron. Soc. Canada 62, 313

Stilburn J.R., Stetson P.B., Fisher W.A., 1992, J. Roy. Astron. Soc. Canada 86, 140

Toner C.G., Gray D.F., 1998, ApJ 334, 1008

Udick S., 1912, Publ. Allegheny Obs. 2, 191

Verschueren W., 1991, Ph.D. Thesis, Free Univ. of Brussels (VUB), Belgium

Verschueren W., David M., 1999, A&AS 136, 591

Verschueren W., David M., Griffin R.E.M., 1999, A&AS 140, 107 (Paper I)